International Journal of Nanomedicine

Dovepress
Taylor & Francis Group

Open Access Full Text Article

ORIGINAL RESEARCH

Chitosan-Based Intelligent Microneedles for Delivery of Amphotericin B Loaded Oleosomes: Antifungal Ocular Patch Targeting for Effective Against Fungal Keratitis Using Rabbit Model via TLR4/NLRP3 Pathway

Sammar Fathy Elhabal[1], Saeed Abdul-Kareem Saeed Al-Zuhairy[2], Mohamed Fathi Mohamed Elrefai[3,4], Mohamed A El-Nabarawi[5], Sandra Hababeh[6], Kristina Zarif Attalla[7], Mai S Shoela[8], Jakline Nelson[9], Marwa Fady[10,11], Nahla A Elzohairy[11,12], Mariam E Amin[13], Heba Sabry Ahmed[14], Tassneim M Ewedah[15], Ibrahim Mousa[16], Ahmed Mohsen Elsaid Hamdan[17]

[1]Department of Pharmaceutics and Industrial Pharmacy, Faculty of Pharmacy, Modern University for Tech-Nology and Information (MTI) Mokattam, Cairo, Egypt; [2]Department of Pharmacy, Kut University College Kut, Wasit, 52001, Iraq; [3]Department of Anatomy and Embryology, Faculty of Medicine, Ain Shams University, Cairo, 11591 Egypt; [4]Department of Anatomy, Physiology and Biochemistry, Faculty of Medicine, The Hashemite Uni-Versity, Zarqa, 13133 Jordan; [5]Department of Pharmaceutics and Industrial Pharmacy, Faculty of Pharmacy, Cairo University, Cairo, Egypt; [6]Department of Pharmaceutics, College of Pharmacy, King Saud University, Riyadh, Saudi Arabia; [7]Department of Pharmaceutics, College of Pharmaceutical Sciences and Drug Manufacturing, Misr University for Science and Technology, Giza, Egypt; [8]Department of Clinical Pharmacology, Faculty of Medicine, Alexandria University, Alexandria, Egypt; [9]Department of Microbiology and Immunology, Faculty of Pharmacy, Nahda University, Beni-Suef (NUB), Beni-Suef, 62511, Egypt; [10]Zagazig University Hospitals, Infection Control Unit, Zagazig, 44519, Egypt; [11]Department of Microbiology and Immunology, Faculty of Pharmacy, Modern University for Technology and Information (MTI) Mokattam, Cairo, 11571, Egypt; [12]Air Force Specialized Hospital, Cairo, 19448, Egypt; [13]Microbiology and Immunology Department, Faculty of Pharmacy, Suez Canal University, Ismailia, Egypt; [14]Department of clinical pharmacology, faculty of medicine, Zagazig university, Zagazig, 44519, Egypt; [15]Pharmaceutics and Pharmaceutical Technology Department, Faculty of Pharmacy, Egyptian Russian University, Cairo, Egypt; [16]Pharmaceutics Department, Faculty of Pharmacy, Sinai University, Al-Arish, Egypt; [17]Department of Pharmacy Practice, Faculty of Pharmacy, University of Tabuk, Tabuk, Saudi Arabia

Correspondence: Sammar Fathy Elhabal, Email Sammar.Fathy@pharm.mti.edu.eg; sammar_fathy2007@yahoo.com; Ahmed Mohsen Elsaid Hamdan, Email a_hamdan@ut.edu.sa

Background: Fungal keratitis (FK), a major cause of blindness, remains challenging to treat due to poor drug penetration and antifungal resistance. Amphotericin-B (AmB), a water-insoluble and low-permeability, necessitates innovative delivery systems to improve its therapeutic efficacy.

Methods: AmB was encapsulated within oleosomes (Ole) prepared using the ethanol injection method, using phosphatidylcholine (Lipoid S100) and sodium oleate, resulting in nanosized spherical globules. The optimized Ole were characterized, then the selected Ole were incorporated into sodium polyacrylate/PEG/chitosan-based microneedles (AmB-Ole/MNs) to improve ocular delivery by creating transient microchannels on the eye surface.

Results: The optimized Ole showed a droplet size of (175 ± 0.78 nm), polydispersity index of (0.33 ± 0.04), zeta potential of (31 ± 0.43 mV), high entrapment efficiency (91±0.63%), and improved stability, bioavailability, and controlled drug release. The AmB-Ole/MNs system increases corneal penetration and contact time via transient microchannels in the eye surface, achieving sustained drug delivery over 72 hours with 70% ex vivo permeation over 80 hours compared to AmB. In vitro antifungal activity and histopathological examination showed that the AmB-Ole/MNs system has potent biofilm disruption (>90%) and 27 mm and 32 mm zones of inhibition against *Candida albicans* and Aspergillus niger, respectively. The Cytotoxicity test showed reduced AmB toxicity with biocompatibility and in vivo *rabbit model*, ocular tolerance by targeting TLR4/NLRP3 pathways and histopathological studies.

Conclusion: The AmB-Ole/MNs system as an innovative ocular delivery platform for fungal keratitis offers sustained drug release, enhanced permeation, potent antifungal activity, and reduced toxicity. AmB-Ole/MNs showed promise for ocular AmB delivery for FK.

Received: 29 December 2024
Accepted: 30 April 2025
Published: 8 May 2025

Keywords: microneedles, fungal keratitis, amphotericin-B, antifungal, chitosan, ocular, *candida albicans*, *aspergillus niger*

Introduction

Fungal keratitis (FK), which results in blindness, accounts for 20–60% of corneal infections with positive cultures in tropical and subtropical areas. Underdeveloped nations report 1.5–2 million cases of keratitis-related blindness annually.[1,2] FK risk factors include corneal injury, prolonged contact lens wear, eye surface disorders, and topical steroid use. Fk affects 1.4 million people worldwide, and 10% of eyeballs perforated, causing monocular blindness in 60%.[3,4] In tropical areas, filamentous fungi like *Fusarium* and *Aspergillus* species cause most of the FK, while yeasts like Candida species are rarer. The biofilm that causes antifungal resistance makes *Candida* spp ocular infections difficult to treat. Management is difficult due to the disease's subtle clinical appearance and poor antifungal response.[5] Mycotic infection must be treated if the presence of leading risk factors like plant-caused corneal damage, indiscriminate topical corticosteroids, or prolonged contact lens use exists.[6]

Topical natamycin therapy is the main treatment for FK, but voriconazole, fluconazole, itraconazole, chlorhexidine, amphotericin B, and econazole can also be used.[7] However, most topical antifungal drops do not penetrate the deeper corneal layers, resulting in insufficient therapeutic concentration at the infection site, a suboptimal therapeutic response, prolonged treatment, and unfavourable outcomes.[1] Therapeutic penetrating keratoplasty (TPK) is performed more often for fungal infections than bacterial keratitis. TPK has a higher graft failure rate than bacterial aetiology. Therefore, an alternative strategy is needed to improve corneal transplant results in stubborn cases.[8,9]

Amphotericin B (AmB) is a broad-spectrum antifungal agent used for the treatment of severe systemic and ocular infections, including candidiasis and aspergillosis. However, its clinical use is often limited by poor solubility and significant toxicity, particularly nephrotoxicity in deoxycholate formulations.[10] Newer delivery systems, such as lipid-based carriers, have aimed to improve their safety and efficacy profile. In the context of fungal keratitis, topical administration of AmB remains suboptimal due to poor corneal permeability and limited ocular retention, highlighting the need for novel delivery strategies.[6] Traditional AmB deoxycholate and lipid-based formulations, such as liposomes, lipid complexes, and colloidal dispersions, optimize efficacy and toxicity for many therapeutic applications. AmB heals cryptococcal meningitis and severe disseminated candidiasis best, but liposomal formulations are preferred by those who cannot tolerate deoxycholate, which is nephrotoxic.[3] AmB can be breathed or injected intraperitoneally to treat organ-specific fungal infections like pulmonary aspergillosis and fungal peritonitis. Due to its broad spectrum and multiple delivery routes, AmB is a versatile antifungal. AmB treats serious eye conditions like fungal keratitis and endophthalmitis. For fungal keratitis, topical AmB (0.15–0.3%) is diluted with sterile water due to the lack of commercial ophthalmic formulations.[11] It works well against *Candida* species but less than natamycin or voriconazole against filamentous fungi like *Aspergillus* and *Fusarium*. Initially, topical medication is administered every 1–2 hours, with frequency reduced as the infection responds. For severe fungal infections, intravitreal injections of Amphotericin B (5–10 μg/0.1 mL) are used to deliver high local drug concentrations directly into the vitreous cavity.[12] This method is effective for Candida-associated endophthalmitis when used with systemic antifungals. In severe or refractory cases, intravenous AmB 0.5–1 mg/kg/day may be used. Nephrotoxicity and electrolyte imbalances limit its systemic use, requiring close monitoring during therapy.[3,6] AmB, especially lipid formulations, treats Leishmania species parasitic infections. This disorder mostly affects the liver, spleen, and bone marrow. AmB may protect bone marrow transplant patients and immunosuppressive patients from fungal infections in high-fungal-exposure situations.[13] AmB treats fluconazole- and itraconazole-resistant fungal infections as a last resort. AmB may treat severe or resistant mucocutaneous *Candida* infections. Mucorales fungi, mostly Rhizopus, Mucor, and Lichtheimia species, cause mucormycosis, or "black fungus", a deadly fungal infection. Immunocompromised people with uncontrolled diabetes, cancer, or corticosteroids are most at risk. AmB is the best mucormycosis treatment because it fights Mucorales.[9,14] Despite its limited use in eye infections, AmB kills microorganisms. Topicals do not penetrate deeper corneal layers, so they do not treat deep keratitis. Without proper dosages, intravitreal injections can cause retinal toxicity, while topical treatment can cause epithelial toxicity. AmB is usually used when natamycin for filamentous fungus or voriconazole fails. Because of its broad-spectrum

efficacy and low resistance to most fungal diseases, AmB, the first successful antifungal drug, is considered the gold standard for treating systemic fungal infections. Candida species, *Aspergillus fumigatus*, Histoplasma capsulatum, and Cryptococcus neoformans all respond to AmB, Although they are classified as a Biopharmaceutical Classification System class (BCS IV), it is unsuitable for oral formulation development due to low water solubility, permeability, and instability in acidic conditions (pH < 2). Thus, only intravenous AmB products are available; parenteral administration would hasten medication onset, but it is inconvenient, necessitates aseptic techniques, causes pain, and costs more.[15] Oral administration is more popular and accepted than parenteral administration because it is simpler to administer, more convenient, and less painful for patients.

Liposomes, solid lipid nanoparticles (SLNs), and nanostructured lipid carriers (NLCs) are among the nanocarriers being studied for the delivery of Amphotericin B; however, these methods have their limitations when it comes to ocular applications. Liposomes are biocompatible, but they can be unstable, and drug leakage can occur.[16,17] Solid lipid nanoparticles (SLNs) and nanostructured lipid carriers (NLCs) exhibit enhanced stability; nonetheless, they present challenges related to low drug loading capacity and restricted penetration through ocular barriers.[18] Oleosomes' deformable lipid bilayer structure, as well as the presence of oleic acid, a well-known permeation enhancer that improves mucosal delivery, influenced their choice. When used in conjunction with microneedles, the system can effectively bypass corneal barriers, extend drug residence time, and maintain drug release. This allows for direct and minimally invasive delivery of the substance to the ocular tissues.[19] This twin approach provides a novel solution to the limitations of conventional nanocarriers for delivering ocular Amphotericin B.[20] By making AmB more soluble in water and shielding it from acidity, they may enhance its oral bioavailability. Unfortunately, the majority of nanocarriers are toxic in vivo and have a limited capacity to load drugs. In 1998, Lee et al created "oleosomes", or oleic acid-integrated liposomes, to fight lipid peroxidation and inflammation.[21] Since then, their permeation-enhancing qualities have led to their use in topical delivery systems and personal care products.

Oleic acid liposomes (Ole) were first proposed in 1973 by Gebicki and Hicks.[22] These are classified as "unsaturated fatty acid vesicles", which consist of both fatty acids along with their ionized species, they are identified by a closed lipid bilayer membrane.[23] These phospholipid carriers reduce the drug's side effects by enhancing its retention in the skin membrane's cells, effectively combating bacterial infections over longer durations. Oleosomes (Ole) have recently sparked interest due to their ability to improve liposome stability and deformability, as well as their inherent anti-inflammatory, antioxidant, and antibacterial properties, which may improve the therapeutic efficacy of certain drugs.[24] As a result, oleosomes may be considered a viable delivery mechanism for managing multiple sclerosis, as they possess intrinsic antioxidant and anti-inflammatory properties, as well as enhanced permeability and stability.

Microneedles (MNs) are a micron-scale technology measuring between 60 and 1000 μm in height, which minimally infiltrates ocular tissue. In ocular medication administration, microneedles create aqueous channels in the cornea, thereby surmounting the corneal barrier and improving ophthalmic drug absorption. Polymeric microneedles, which are made of biocompatible or biodegradable polymers that reduce ocular tissue damage, allow for recovery in 24 hours and produce no medical waste when fully degraded.[25,26] Various micro- or nanoparticle drug delivery systems have been successfully incorporated into microneedles to improve solubility, bioavailability, or localized delivery. For instance, rapamycin has been delivered via microneedles using a cumbersome (lipophilic) carrier system, while curcumin has been formulated as a nanosuspension, and itraconazole as nanocrystals.[27,28] All demonstrating the microneedle platform's versatility in handling drugs with challenging physicochemical properties.[29]

This research explored the possibility of using AmB nanosized carriers to improve drug delivery to the eyes. Thus, the goal of this study was to improve the ocular delivery of AmB by loading it into Oleosomes and then incorporating it into chitosan-based microneedles. To achieve this goal, AmB-Ole/MNs and AmB-Ole were prepared using the 33 Box-Behnken design to investigate the effect of different formulation variables (Lipoid S100 amount, sodium oleate amount, amphotericin-B concentration) on oleosome properties (including particle size (PS), polydispersity index (PDI), entrapment efficiency percentage (EE%), and zeta potential (ZP)). Afterwards, the selected Oleosomes system was further optimized via incorporation into sodium polyacrylate/PEG/chitosan microneedles, to prolong the contact time with ocular tissues, reduce the elimination of the formulation from ocular tissues and enhance adhesion to the eye surface. According to the literature, chitosan has low ocular toxicity and is well tolerated. In addition, antifungal, cytotoxicity, in vivo, and

biomarker studies were performed to confirm the retention of the drug on the eye surface and ensure the safety and biocompatibility of the tested formulations after ocular application to albino rabbits.

Materials and Methods

Materials

The following products were purchased from Sigma-Aldrich (Milan, Italy): Amphotericin-B, Chitosan (CS, Mw = 300,000, deacetylation degree~85%), Lipoid S100, sodium oleate sodium polyacrylate, PEG 5000, acetic acid, and dimethyl sulfoxide (DMSO). All the solvents were acquired from VWR in Milan, Italy, and were of the reagent or HPLC quality. Medical International Ltd. (London, UK) provided the dialysis membranes (molecular weight cut-off, MWCO: 3500 Da) used in the in vitro release tests.

Methods

Preparation and Optimization of Amphotericin-B Oleosomes (AmB-Ole)

Oleosomes were synthesized utilizing a modified ethanol injection method referred to as AmB-Ole. AmB, Lipoid S100 (l-α-phosphatidylcholine), and sodium oleate were solubilized in 2 mL of absolute ethanol. The ethanolic solution was subsequently injected into a 10 mL methanol/ethanol mixture (1:1 v/v) and mixed using a vortex mixer until clarity was achieved.[30] Table 1 shows that the formed solution was injected into 10 mL of PBS pH = 7.4 at 60°C, and the resulting milky dispersion was stirred at room temperature with a magnetic stirrer at 600 rpm for at least 1 hour to remove the solvent. The formulation was sonicated at 30% amplitude for two cycles of 8 seconds each, followed by an 8-second stop. The goal was to make it smaller. Figure 1 shows that the dispersion was hermetically sealed and refrigerated overnight at 4 °C before being further characterized. The formulation's physical appearance, zeta potential, particle size (PS), and polydispersity index (PDI) were recorded.[24,31]

Physicochemical Characterization of Oleosomes

Entrapment Efficiency

One milliliter of each formulation was subjected to centrifugation at 4000 rpm for 15 minutes utilizing CENTRISART™ ultrafiltration tubes (MWCO 100,000).To ensure accurate separation of free drug, a control experiment was conducted by filtering a known concentration of free AmB under the same conditions. Recovery exceeded 95%, confirming the ultrafiltration method's efficiency for quantifying unentrapped drug.[32] The filtrate indicating the unentrapped concentration was assessed via High-Performance Liquid Chromatography (HPLC) analysis using a C18 column (reverse-phase) measuring 250 mm × 4.6 mm with a 5 µm particle size (Phenomenex, USA). The mobile phase is composed of acetonitrile, methanol and phosphate buffer in a 40:30:30 ratio, has been adjusted to a pH of 7.4 and is flowing at a rate of 1.0 mL/min.[33,34] A correlation coefficient of 0.9996 was obtained by UV detection at the maximum absorption

Table 1 Box-Behnken Statistical Design for Optimization of Amphotericin-B

Factors (Independent Variables)	**Levels**		
X_1: Lipoid S100 amount (mg)	150	200	250
X2: sodium oleate amount (mg)	15	30	40
X3: Amphotericin-B concentration (%)	0.5	1	1.5
Responses (Dependent variables)	**Constraints**		
Y_1: EE (%)	Maximize		
Y_2: PS (nm)	Minimize		
Y_3: PDI	Minimize		
Y_4: ZP	Maximize (absolute value)		

Abbreviations: EE%, entrapment efficiency percent; EA, Edge activator; PS, particle size; PDI, polydispersity index; ZP, zeta potential.

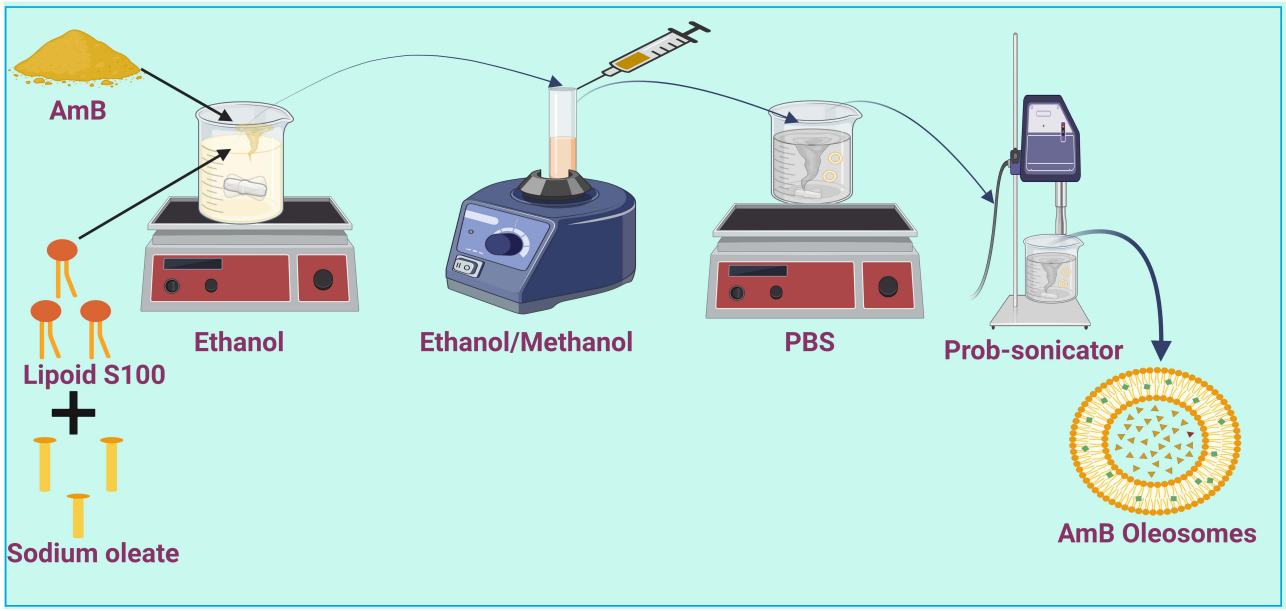

Figure 1 Schematic representation of the fabrication process for Amphotericin-B loaded Oleosomes.

wavelength for AmB, which is approximately 410 nm. The quantification of AmB concentration was achieved through the creation of a standard calibration curve spanning the concentration range of 5 to 200 µg/mL. Consistent performance was ensured by an injection volume of 20 µL at 25–30°C, and the entrapment efficiency was assessed as follows.[35,36]

$$EE\% = \text{Total amount of unentrapped AmB} / \text{total amount of AmB} \times 100 \quad (1)$$

Particle Size, Polydispersity Index & Zeta Potential

The prepared nano-nucleosomes were visually examined for the presence of aggregations or drug precipitation. The solution was subsequently diluted with deionized water and subjected to sonication for 30 seconds. Particle size, polydispersity index, and zeta potential were measured using the Malvern Zeta Sizer Nano ZS (Malvern Instruments, Worcestershire, UK) with a dynamic light scattering particle size analyzer at 25 °C.[37]

Characterization of Optimum Oleosomes

Transmission Electron Microscopy (TEM)

A morphological examination of selected oleosomes was conducted to confirm the vesicular structure utilizing a Transmission Electron Microscope (TEM) (JEM-100S microscope; JOEL Ltd., Tokyo, Japan). Initially, the chosen formula underwent dilution with deionized water and was subjected to sonication for 30 seconds. Subsequently, each sample was positioned on a carbon-coated copper grid and subjected to staining with uranyl acetate. The surplus stain was eliminated, and the samples were allowed to dry before imaging.[38]

Fourier Transform Infrared (FTIR) Spectroscopy

FTIR spectra were collected for AmB, the Ole blank without AmB, and the optimal AmB-Ole formulation. Dry potassium bromide was mixed with approximately 2–3 mg of each sample and then pressed into a disk before scanning in the range of 4500–500 cm^{-1} at room temperature.[39]

Differential Scanning Calorimetry (DSC)

The melting point of all samples was assessed using differential scanning calorimetry (DSC N-650 model, Science, Seoul, Korea) to analyze the interaction between the medication and excipients. In summary, 3–5 mg of the differential

https://doi.org/10.2147/IJN.S514798

Table 2 Fabrication of Sodium Polyacrylate-PEG/Chi-MNs Loading Lyophilized Amphotericin-B -Oleosomes

Formulation	SP	PEG-5000	Chi
M1	3	15	10
M2	6	10	15
M3	9	5	25

Abbreviations: SP, sodium polyacrylate; PEG, Polyethylene Glycol; Chi, chitosan; MNs, Microneedles.

scanning calorimetry (DSC) formulations was analyzed in an aluminium pan. The experimental setup included a temperature range of 24 to 350 °C, with a heating rate set at 10 °C/min.[40,41]

Stability of Lyophilized Powder

The optimized oleosomes were subjected to lyophilization. Mannitol was added to the coated nanovesicles to reach a final concentration of 5%. The formulation was frozen at −80 °C for 24 hours before being transferred to the lyophilizer. Lyophilization was performed at a pressure of 40 mbar and a temperature of −65 °C. The collected powder was stored in a desiccator with $CaCl_2$ at room temperature before testing. A portion of the powder was used to fabricate microneedles, while the remaining portion was reconstituted in PBS at pH 7.4 after three months. The samples were subsequently analyzed for their physicochemical properties.[37,42]

Fabrication of Crosslinked Hydrogel-Forming Chitosan-Based Microneedles Patch

The composition of the crosslinked hydrogel patch was adapted from earlier research, combination of sodium polyacrylate (serving as a crosslinker) and PEG 5000 (acting as a plasticizer) was dissolved in deionized water and agitated overnight. Chitosan utilized as a polymer, was synthesized by dissolving it in a 0.1% acetic acid solution and agitating overnight. Two polymer solutions, each containing 10 mL of lyophilized ole with AmB (equivalent to 40 mg of AmB), were combined to attain a 1:1 weight ratio. The mixture was subsequently poured into square silicone molds. The molds were vacuumed for about 10–15 minutes to remove any trapped air and ensure that the microcavities were completely filled. After 48 hours of drying at room temperature, the molds were thermally crosslinked. This vacuum-assisted casting step helped to improve microneedle uniformity and reduce air pockets.[43] Subsequently, the dried hydrogel patches were removed and thermally crosslinked at 80–100 °C for 30–60 minutes, as specified by the experimental design, as illustrated in Table 2 and Figure 2.

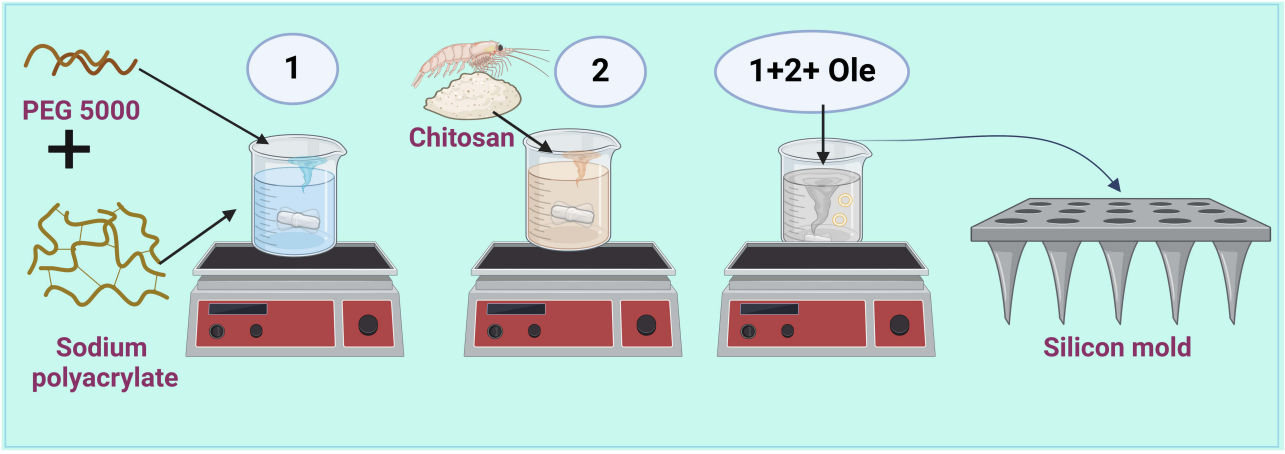

Figure 2 Schematic representation of the Microneedle fabrication process for Amphotericin-B loaded Oleosomes.

Evaluation of AmB-Ole/MN Patch

Studies on Drug Content

Distilled water with 2.5% Tween 80 was utilized to dissolve a selection of optimized AmB-Ole/MNs in magnetic agitators at a stirring speed of 300 rpm for one hour. The resultant solution was diluted with 1 mL of dimethyl sulfoxide (DMSO) to augment the solubility of amphotericin B (AmB), and this solution was subsequently mixed with acetonitrile to precipitate the polymer. The supernatant obtained from centrifugation of this dispersion at 12,000g for 10 minutes was subsequently utilized to permit the AmB from the synthesized AmB-Ole/MNs to be injected into the previously validated HPLC method outlined in previous section. The drug content of the manufactured MNs was determined through triplicate studies, with the data presented as drug weights per MNs array (mean ± SD, n = 3).[35,44]

Mechanical Characterization

Weights of 250 g, 500 g, and 1000 g were applied to the tips of the AmB-Ole/MNs patch for five minutes before removal for the measurement of the DMN's height reduction. The structure and fracture of the optical microscope were subsequently employed to evaluate the DMNs, demonstrating their mechanical strength. The tip diameter, base diameter, and length of three arrays of AmB-Ole/MNs were quantified using a microscope. The aspect ratio is determined by dividing the length by the base diameter ratio.[45] All calculations were performed in triplicate, and the mean ± standard deviation was determined.

Characterization of Optimized Microneedles

Scanning Electron Microscopy (SEM)

The morphology of the AmB-Ole/MNs patch was examined utilizing a scanning electron microscope (SU8010, HITACHI, Japan). The AmB patch was attached to a microscope carrier, and imaging was performed at 6 kV with a magnification of 150×.[46,47]

Fourier Transform Infrared (FTIR) Spectroscopy

FTIR spectra were obtained for MNs blank without AmB-Ole, and the optimum MNs1 formula, by the same method mentioned before.

Differential Scanning Calorimetry (DSC)

DSC were obtained for MNs blank without AmB-Ole, and the optimum MNs1 formula, by the same method mentioned before.

Saturation Solubility Study

A saturation solubility study was conducted to determine the optimal dissolution medium for Amphotericin B. Excess amounts of pure AmB were added to 10 mL of different solvent systems, including distilled water, phosphate buffer (pH 7.4), ethanol, and ethanol-water mixtures at various ratios (10:90, 30:70, 50:50 v/v). The suspensions were sonicated for 5 minutes and then shaken at 37 ± 0.5 °C for 48 hours in a thermostatically controlled shaking water bath. After equilibration, samples were filtered through a 0.45 μm membrane filter and analyzed by HPLC. The ethanol-water mixture (30:70 v/v) showed the highest solubility and was selected as the release medium for subsequent in vitro drug release studies.

In vitro Drug Release Study

The in-vitro release of AmB solution, AmB-Ole, and AmB-Ole/MNs was conducted utilizing the dialysis bag method (visking® 28 mm, MWCO 12,000–14,000; Serva, Heidelberg, Germany). The experiment was conducted in a thermostatically controlled shaking water bath maintained at 37 ± 0.5 °C and 60 rpm, utilizing a 10 mL in ethanol/water mixture (30:70 v/v), which was selected based on preliminary saturation solubility studies showing significantly enhanced solubility of AmB in this medium. This solvent system was chosen to maintain sink conditions during the in vitro release assay while minimizing the use of organic solvents. After 0.25, 0.5, 1, 2, 4, 6, 12, 24, 48, 72, and 80 hours, the complete volume of the release medium was extracted and substituted with an equivalent volume of fresh media, which had been preserved at the same temperature.[32] HPLC was used to compare each sample to a blank made of ethanol and water mixed in a 30:70 ratio. The release test was also done on blank

formulations, and the release medium was taken out at the same time each time to act as a blank for the sample measurements. Three copies of each experiment were done, and the results were given as the mean ± S.D.[48,49]

Ex vivo Permeation Study

We tested the ex vivo penetration of AmB-Ole, AmB-solution, and AmB-solution/MNs in corneal tissue from sheep obtained from a nearby Cairo, Egypt, slaughterhouse. To measure the amount of AmB in the cornea, a microbiological assay method that has been validated was used. Using a modified Franz diffusion cell apparatus, the ocular penetration of different AmB formulations was evaluated ex vivo. An ocular AmB solution equivalent to the drug, AmB-Ole, along with AmB-Ole/MNs, was administered to the surface of the sheep's cornea positioned in the diffusion cell. Water maintained at 37 °C circulated through the water jacket encasing the receptor cell, while a Teflon-coated magnetic stir bar positioned at the bottom of the receptor cell facilitated uniformity in the receptor volume. The diffusion medium consisted of phosphate buffer at pH 7.4 was used to closely simulate the physiological tear fluid environment. A sample of receptor media was collected at specified time intervals (1, 2, 4, 6, 8, 24, 48, 72, and 80 hours), and the concentration of AmB was quantified. Following 80 hours, the cornea was extracted from the cell and homogenized with 5 mL of DMSO for 5 minutes.[50,51]

Cytotoxicity Assay

Immortalized human keratinocyte HaCaT keratinocytes from the American Type Culture Collection (ATCC Manassas, VA, USA) (ATCC PCS-201–012) supplemented with 10% fetal bovine serum and 1% penicillin-streptomycin, at 37 °C in a 5% CO_2 humidified incubator. Cells were seeded in 96-well plates at a density of 1×10^4 cells/well and allowed to adhere overnight (Thermo Fisher Scientific Co.) at 37 °C in a humidified environment with 5% CO_2.

For the assay, AmB, AmB-Ole, and AmB-Ole/MNs formulations were freshly prepared in sterile DMEM to achieve final AmB concentrations ranging from 1 to 20 μg/mL. For MNs, the patches were pre-dissolved in DMEM and filtered before application. The cells were then treated with 100 μL of each formulation for 48 hours.[52,53] After the incubation period, 20 μL of MTT reagent (5 mg/mL) was added to each well and incubated for 4 hours. Formazan crystals were then solubilized using 100 μL of DMSO, and absorbance was measured at 570 nm using a microplate reader. Cell viability was calculated relative to untreated control wells, and each condition was tested in triplicate. Micelles were diluted in DMEM media and added to 96-well plates with 1×10^4 cells per well. Survival rates (0% and 100%) were determined following treatment with 0.3% (v/v) Triton X-100 or DMEM, respectively, the results were expressed as mean ± SD.[54]

In vitro Antifungal Activity

Agar Disc Diffusion Technique

According to the National Committee for Clinical Laboratory Standards (NCCLS) guidelines, the agar disc diffusion method was used to assess the antifungal efficacy of the AmB, Ole blank without AmB, AmB-Ole, and AmB-Ole/MNs.[55] Fungal strain suspensions were made, and using a spectrophotometer set to 570 nm, the turbidity was adjusted to reach a final concentration equal to a 0.5 McFarland standard. The potato's surface was covered with a sterile disc that contained 0.1 mL of each drug formulation at a concentration of 200 g/100 L of AmB-Ole/MNs (0.2% w/v), and a fungus strain was added to dextrose agar plates. Fluconazole discs served as the control, while the AmB solution and the Ole blank served as the blank. To promote diffusion, the plates were left to stand for 30 minutes before being incubated for 24 to 48 hours at 37 °C. Millimetres were used to measure the diameter of the inhibition zones encircling the wells for the potential eradication of ocular fungal infections.[8]

Determine the Minimum Inhibitory Concentration (MIC)

The CLSI broth microdilution technique was employed to ascertain the minimum inhibitory concentration for AmB, Ole devoid of AmB, AmB-Ole, and AmB-Ole/MNs against the evaluated fungal strains. The tested concentration range for AmB was 0.031 to 16 μg/mL. To execute the two-fold serial dilutions, the drug formulations were initially dissolved in 50 μL of dimethyl sulfoxide (DMSO). The prepared doses were positioned in a 96-well microplate containing 100 μL of Sabouraud Dextrose broth. Each well received 50 μL of fungal suspension at an approximate concentration of 106 mL^{-1}. The microplate underwent incubation for 48 hours at 28 degrees Celsius. The highest degree of dilution yielded a

minimal inhibitory concentration, leading to the absence of fungal growth. To guarantee precise outcomes, MIC measurements were conducted in triplicate.[52,56]

Determine the Minimum Bactericidal Concentration (MBC)

The Minimum Bactericidal Concentration (MBC) is calculated by plating and counting the dilution that corresponds to the Minimum Inhibitory Concentration (MIC) as well as at least two higher concentrations of the test product to assess viable colony-forming units per milliliter (CFU/mL). The minimum bactericidal concentration (MBC) is the lowest concentration that results in a specific reduction in colony-forming units per milliliter (CFU/mL) when compared to the minimum inhibitory concentration (MIC) dilution, such as 99.9%.[57]

Antibiofilm Assay and Crystal Violet Staining (CVS) Assay

The 96-well microtiter plate was divided into four groups, each containing a mixture of serially diluted AmB, a control without AmB, AmB-Ole, and AmB-Ole/MNs. The final well functioned as a negative control. In each well of the microplate, 300 µL of fresh trypticase soy yeast broth (TSY) was dispensed, achieving a final concentration of 106 CFU/mL, and cultured with previously established sublethal concentrations (75%, 50%, and 25% of MBC). Wells containing medium and those lacking extracts, which contained only methanol, functioned as controls. Plates were incubated at 37 °C for 48 hours. Following incubation, the supernatant was removed, and each well was extensively rinsed with sterile distilled water to eliminate any free-floating cells. The biofilm underwent staining with a 0.1% aqueous solution of crystal violet for 15 minutes at ambient temperature, after a 30-minute air-drying interval of the plates. The plate was rinsed three times with sterile distilled water to remove excess stains after incubation.[58,59] Each well was administered 250 µL of 95% ethanol to solubilize the dye within the cells. Absorbance was recorded at 560 nm using a microplate reader after a 15-minute incubation period.

$$(\text{Control OD} - (\text{Sample OD}/\text{Control OD})) \times 100 \quad (2)$$

Control OD represents the absorbance of the negative control, while Sample OD denotes the absorbance of the test sample.

In vivo Studies

Animals

In this study, healthy 36 adult male New Zealand albino rabbits were examined for any health problems (the animals weighed between 2–2.5 kg, were 4–6 weeks old, had bright fur, no discharge, dullness, or scratching on the cornea in either eye, or twitched their noses regularly). The rabbits were kept in a temperature-controlled environment (22–25 °C) with a 12-hour light/dark cycle and free access to food and water. All animal experiments were carried out with the approval of the Research Ethics Committee for Experimental and Clinical Studies at the Faculty of Pharmacy, Cairo University, Egypt (Approval no. PI3413), under the local and national regulatory standards for animal care established by Cairo University's animal care committee.

Eye Irritation Test (Draize Test)

This experiment included six rabbits, divided into two groups of three rabbits each, to assess the irritancy of the optimized formula. The initial group was administered the optimal AmB-Ole, while the subsequent group received M1, the optimal Microneedle. Two drops (100 µL) of the tested formula, equivalent to 400 µg of AmB, were administered in the conjunctival sac of the left eye. Saline was administered at intervals of 0, 1, 2, 3, 4, 5, 6, 24, 48, and finally at 72 hours, followed by applications at 7, 14 and 21 days post-installation, with the right eye designated as a control. The irritation grade of each rabbit eye was evaluated. Post-delivery, the ocular irritation score was assessed upon achieving a zero value at a specified interval. Ocular irritation was evaluated based on the Draize scoring system, which assesses conjunctival redness, chemosis, and discharge on a scale of 0 to 3 (0 = none, 1 = mild, 2 = moderate, 3 = severe). Scores were recorded at 1, 24, 48, and 72 hours post-application(indicating maximum redness and irritation).[60–62]

In-vivo Antifungal Activity of AmB Formulations (Susceptibility Test)

This test aimed to evaluate the antifungal efficacy of the assessed AmB formulations. The organism used in this experiment was *Candida albicans* ATCC 10221. Following the administration of a 50 µL aliquot (0.2% w/v AmB) of the tested formulations into the conjunctival sac of the right eyes of nine male albino rabbits **Group 1**: Healthy control; **Group 2**: Untreated negative control; **Group 3**: AmB solution. **Group 4**: Optimized AmB-Ole; **Group 5**: AmB-Ole-MNs. Five sterile filter paper discs, approximately 6 mm in diameter, were moistened by placing the discs beneath the eyelid of each eye for approximately 1 minute at designated time intervals over 12 hours. No drug was administered to the left eye to serve as a control. Two discs were introduced into 500 µL of Sabouraud dextrose broth (SDB) and inoculated with a 10% v/v yeast suspension (10^6 CFU/mL). The remaining two discs were immersed in 500 µL of uninoculated SDB to measure optical densities, serving as a blank. The broths were incubated at 25 ± 2 °C for 24 hours under aerobic conditions. Following incubation, 200 µL of each broth was transferred to a sterile 96-well plate. Optical densities (OD 570nm) were measured using an automated spectrophotometric plate reader (Biotek, Synergy 2, USA) at a wavelength of 570 nm. The results were presented as the mean growth inhibition percentage (mean ± SE).[35,58] The percentage of growth inhibition was determined using the following equation:

$$\text{Growth inhibition}\,\% = \frac{Control\ (left\ eye)OD\ 570\ nm - \ \times\ Test\ group(rigth\ eye)OD\ 570\ nm}{Control(left\ eye)OD600\ nm} \times\ 100 \qquad (3)$$

Assessment of Inflammatory Biomarkers

Each rabbit was anaesthetized with pentobarbital sodium (200 mg/kg, IP) 24 hours following the most recent treatment, and blood samples were collected via the retro-orbital sinus. The manufacturer's instructions were followed to analyze the serum for NLRP3 (NOD-, LRR-, and Pyrin Domain-Containing Protein 3), IL-6 (Interleukin-6), TNF-α (Tumor Necrosis Factor-Alpha), IL-1β (Interleukin-1 Beta), and TLR4 (Toll-Like Receptor). MyBioSource, located in San Diego, California, USA, provided this enzyme-linked immunosorbent test (ELISA) kit.[63,64]

Histological Examination

Following pharmacodynamic testing, rabbits were injected with phenobarbital sodium in a marginal vein, which caused death. Following the removal of the eyeballs, 10% formalin was given. The thin cornea, sclera, and ciliary body sections were prepared by cutting, cleaning, and dehydrating in xylene. The materials were dehydrated, clarified, sealed in paraffin blocks, and sectioned to a thickness of 4–6m. The acquired tissue samples were histologically evaluated using an electric light microscope after H&E staining and xylol deparaffinization.[65,66]

Data Statistical Analysis

The one-way analysis of variance (ANOVA) test was used to determine whether there was a significant difference between the formulas' results. The level of significance was set at 0.05 ($p < 0.05$).

Results and Discussion

Formulation Optimization (EE%, PS, PDI, and ZP)

The study sought to improve oleosome formulations for AmB by examining the effects of three main factors: Lipoid S100 quantity (X1), sodium oleate amount (X2), and AmB concentration (X3). The measured responses were entrapment efficiency (EE%, Y1), particle size (PS, Y2), polydispersity index (PDI, Y3), and zeta potential as shown in Table 3 and Figure 3.Entrapment Efficiency (EE%, Y 1): The EE varied from 67% (Ole-1) to 91% (Ole-10).

Higher concentrations of Lipoid S100 (X1), such as 250 mg, markedly enhanced encapsulation efficiency (EE) by facilitating superior oleosome bilayer formation. Ole-10 (250 mg once) demonstrated maximum encapsulation efficiency. Sodium oleate (X2) with moderate concentrations (eg, 30 mg in Ole-10) enhanced encapsulation efficiency, presumably due to its function as a stabilizer and edge activator, hence enhancing vesicle production. Moderate to high quantities of Amphotericin-B (X3) ranging from 1% to 1.5% yielded favourable encapsulation efficiency, indicating efficient

Table 3 Experimental Runs, Independent Variables, and Measured Response of the 3^3 Full Factorial Experimental Designs of Amphotericin-B-Oleosomes (AmB-Ole)

Code	Factors			Responses			
	X1:Lipoid S100 amount (mg)	X2: sodium oleate amount (mg)	X3:Amphotericin-B concentration (%)	Y1: EE (%)	Y2: PS (nm)	Y3: PDI (nm)	Y4: ZP (mV)
Ole-1	150	15	0.5	67±0.21	531±0.72	0.71±0.03	28±0.76
Ole-2	150	40	1.5	69±0.55	310±0.56	0.67±0.02	26±0.06
Ole-3	200	30	0.5	74±0.23	551±0.40	0.72±0.07	23±0.12
Ole-4	250	15	0.5	83±0.41	561±0.87	0.31±0.11	36±0.43
Ole-5	250	40	1	87±0.21	354±0.45	0.76±0.06	29±0.32
Ole-6	150	30	1	68±0.32	601±0.62	0.56±0.04	31±0.54
Ole-7	200	15	1	71±0.41	512±0.43	0.43±0.02	38±0.52
Ole-8	150	30	1	81±0.39	596±0.67	0.45±0.12	26±0.45
Ole-9	250	40	0.5	87±0.61	353±0.76	0.54±0.14	24±0.62
Ole-10	**250**	**30**	**1**	**91±0.63**	**175±0.78**	**0.33±0.04**	**31±0.43**
Ole-11	250	30	1.5	85±0.34	473±0.43	0.67±0.05	30±0.63
Ole-12	150	15	1.5	82±0.71	598±0.33	0.69±0.07	34±0.49
Ole-13	200	15	1	69±0.77	501±0.51	0.91±0.05	33±0.67
Ole-14	200	15	0.5	72±0.54	524±0.92	0.45±0.03	31±0.29
Ole-15	200	40	1.5	70±0.58	341±0.65	0.87±0.12	25±0.48

Abbreviations: AmB-Ole, Amphotericin-B-Oleosomes; EE%, entrapment efficiency percent; PS, particle size; PDI, polydispersity index; ZP, zeta potential; bolded means optimized formula(Ole-10).

encapsulation without oversaturation. The findings indicate that the interactions and quadratic effects of the components significantly influence entrapment efficiency, with AmB concentration (X3) exerting the greatest effect.[37] Formulations Ole-5, Ole-9, and Ole-10 exhibit elevated EE values (87–91%) owing to optimal X3 levels and beneficial interactions between X1 and X2. Underlines the significance of these interactions, implying that raising X3 enhances EE up to a point when drug leakage occurs, as evidenced by declines in EE at greater extrusion cycles or drug concentrations.

$$EE\%=86.33-0.62X1+0.45X2+69.02X3+0.01X1X2-0.35X1X3+0.65X2X3+0.01X12-0.07X22-5.53X32$$

Particle Size (PS, Y2): The particle size decreased with reductions in X1, X2, and X3, as illustrated by the following equation: $Y2=903.9036-1.1639X1-5.6561X2-53.3425X3$

This tendency is consistent with the findings for formulations Ole-2, Ole-5, and Ole-10, which showed lower particle sizes (175–354 nm) at higher X2 levels and moderate X1 and X3 levels. The reduced PS can be attributed to sodium oleate's surfactant characteristics and the improved drug concentration, both of which stabilize the vesicles and prevent aggregation varying from 225 nm (Ole-10) to 601 nm (Ole-6). Lipoid S100 (X1), increased quantities decreased PS, likely attributable to enhanced bilayer formation and stabilization. Sodium oleate (X2) with elevated doses (40 mg in Ole-9) produced diminutive vesicles, presumably attributable to improved emulsification characteristics.[24,38] The concentration of Amphotericin-B (X3) with Elevated concentrations appeared to enhance PS (eg, Ole-12, 598 nm), indicating drug-induced aggregation. Increasing the concentration of Amphotericin B (X3) initially increased entrapment efficiency because more drug was available for incorporation into the lipid bilayer. However, as concentrations increased, EE% decreased. This could be due to vesicle saturation, in which the lipid bilayer is unable to accommodate more drug molecules. Excess AmB can accumulate on the vesicle surface, causing membrane destabilization, phase separation, or steric hindrance, which can promote drug leakage or aggregation. Similar behavior was observed in other nanosystems loaded with highly lipophilic drugs.

Polydispersity Index (PDI; Y3): PDI scores varied from 0.31 (Ole-4) to 0.91 (Ole-13) as illustrated by the following equation: $PDI=0.6047$. Lipoid S100 (X1) which increased quantities enhanced homogeneity (eg, Ole-4, 250 mg X1). Sodium oleate (X2) with both excessively low and high concentrations elevated PDI, signifying irregular particle production. Moderate concentrations of Amphotericin-B (1%) yielded excellent photodynamic inactivation, indicating stable vesicle formation. The parameters did not appear to have a significant effect on PDI values, indicating that the process settings, such as the ethanol injection method. This stability is evident in the low variation in PDI amongst formulations, which ranges from 0.31 to 0.91. Ole-4 (0.31) and Ole-10 (0.33) showed the best homogeneity.The selected

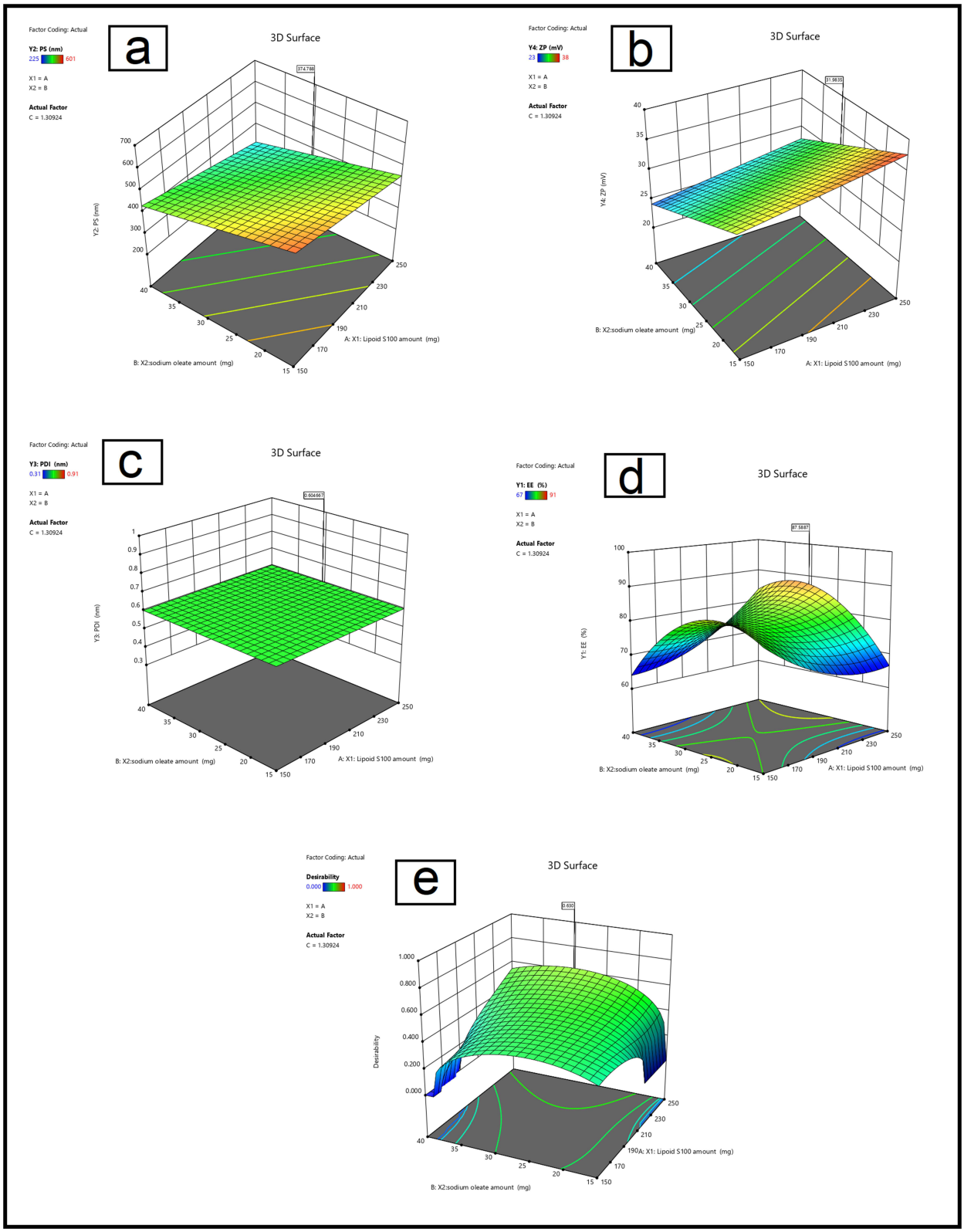

Figure 3 Response 3D plots for the effect of (X1) Lipoid S100 amount, (X2) sodium oleate amount, (X3) Amphotericin-B concentration, on (**a**) Entrapment Efficiency %, (**b**) Particle Size (**c**) Polydispersity index (**d**) Zeta Potential, and (**e**) Dispersity.

AmB-Ole formulation had a slightly higher PDI value (0.33 ± 0.04) due to AmB amphiphilic structure, which can lead to aggregation. Such behavior can cause partial heterogeneity during vesicle formation. Furthermore, the ethanol injection method, while convenient and scalable, can produce vesicles of different sizes depending on the mixing rate and solvent removal efficiency. Despite this, the formulation demonstrated acceptable stability and entrapment efficiency.

Zeta Potential (ZP or Y4): ZP readings varied from 23 mV (Ole-3) to 38 mV (Ole-7) as illustrated by the following equation: ZP=27.7702+0.0385X1−0.3849X2+4.6182X3

Lipoid S100 (X1) increased quantities resulted in more stable formulations (eg, Ole-7, 38 mV), presumably due to augmented lipid bilayer integrity. Sodium oleate (X2) with moderate concentrations enhanced stability (Ole-10, 31 mV), whereas excessive amounts diminished Zeta potential.[37,63] Amphotericin-B concentration (X3) with higher concentrations decreased ZP, possibly due to increased drug content affecting surface charge X3 had the strongest influence on the zeta potential, the negative zeta potential was increased because of interactions between the medication and the phospholipid bilayer which occurred when the concentration of AmB was increased. Specifically, this pattern was observed in formulations such as Ole-4 and Ole-7, where the presence of high X3 levels resulted in large increases in ZP. The fact that oleic acid produces an increase in the accumulation of negative charge lends credence to the theory that it raises surface charge and increases AmB concentration from 0.1% to 0.5% lowering PS and ZP while increasing EE. These results indicate that AmB is solubilized within the bilayer and interacts with oleic acid, causing vesicle constriction and enhanced entrapment. However, excessive drug loading resulted in precipitation, as demonstrated by 0.5% AmB. Nevertheless, elevated drug loading led to precipitation, as shown with 0.5% AmB. Classic liposomes without oleic acid had bigger particle sizes, lower ZP, and lower EE than oleosomes. The inclusion of oleic acid improved the vesicles' surface characteristics and stability, as evidenced by previous research on the impact of surfactants in decreasing surface tension. The optimized oleosome formulation (Ole-10) showed the best balance of EE, PS, PDI, and ZP, making it a good option for further development.[67]

Physicochemical Characterisation of Optimum Oleosomes

Transmission Electron Microscopy (TEM)

Figure 4a. showed morphological examination of selected oleosome was performed on the AmB-Ole. Spherical nanovesicles with dark cores and brightened edges were identified. TEM analysis results are remarkably consistent with previously determined PS readings.[68,69]

Fourier Transform Infrared (FTIR) Spectroscopy

As shown in Figure 4b, the FTIR spectra pure AmB have typical peaks of Amphotericin B, such as strong absorptions around 1650 cm^{-3} (indicating that the amide group is stretching from C=O to N–H) and 1550 cm^{-3} (indicating that the amide group is bending from N–H to C=O), which are signs of secondary amides. The broadband observed near 3400 cm^{-3} is attributed to O–H stretching vibrations, indicating that AmB contains hydroxyl groups. The peaks at 2930 cm^{-3} and 2850 cm^{+3} are caused by the aliphatic chains' C–H stretching vibrations.[40] DSC analysis of pure AmB showed a sharp endothermic peak at 170°C and a more general event at 290°C, indicating thermal degradation and the melting point. The drug's sharp melting peak and lack of broadening suggest that it interacts little with other components in its native state and maintains its crystalline form. In contrast, the AmB-Ole and microneedle formulations showed modified thermal behavior, indicating encapsulation and potential interaction with the lipid and polymeric matrices. In contrast, the AmB-Ole and microneedle formulations showed modified thermal behavior, indicating encapsulation and possible interaction with the lipid and polymeric matrices. OleBlank includes oleosomes and has features of oleosomes, with strong peaks at 2920 cm^{-3} and 2850 cm^{-3}.[70,71] These peaks show that aliphatic hydrocarbons are present, which means that fatty acids and lipids are running from C to H. There is a broad peak near 3400 cm^{-3} that points to O–H stretching vibrations. These vibrations probably come from the lipid parts and the water molecules. This sample does not contain AmB because it does not show the characteristic AmB peaks (1650 cm^{-3} and 1550 cm^{-3}). Ole10 contains both oleosomes and Amphotericin B can be seen in the blue range. The amide I and II bands at 1650 cm^{-3} and 1550 cm^{-3} show that AmB has been added to the oleosomes. The lipid-associated peaks (2920 cm^{-3} and 2850 cm^{-3}) are still very strong, which proves that the oleosomes are made of fat. The broad O–H peak around 3400 cm^{-3} is a little off or wider

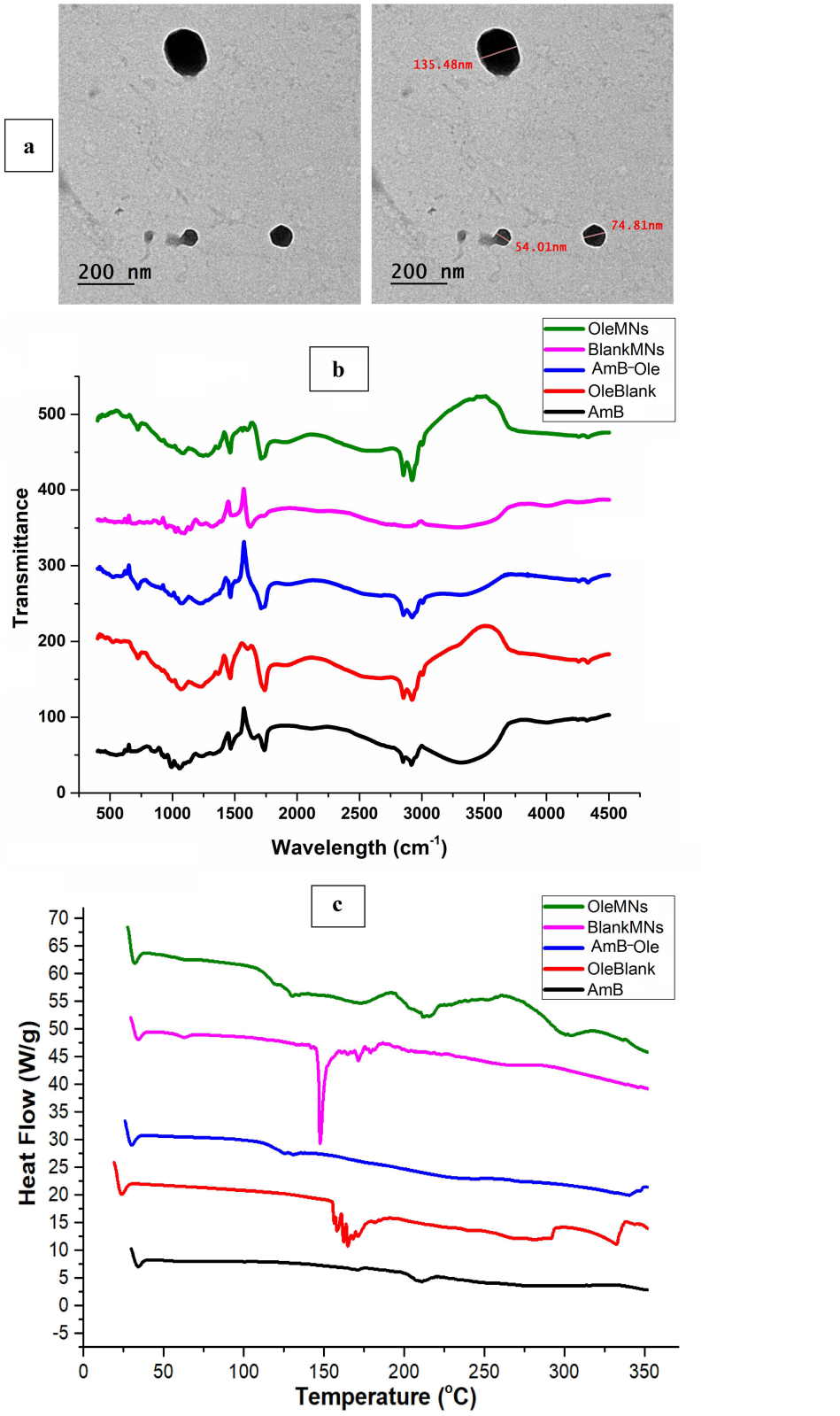

Figure 4 (**a**).Transmission electron microscopy, (**b**). Fourier transform infrared (FTIR) spectroscopy, and (**c**) Differential scanning calorimetry for Amphotericin-B formulations.

than it was in OleBlank. This could mean that Amphotericin B is hydrogen bonding with the lipid framework of the oleosomes.[24,58,63] The development of delivery systems necessitated an understanding of polymer-drug interactions. Thus, it was imperative to use computational tools to examine these connections concurrently.

Differential Scanning Calorimetry (DSC)

As shown in Figure 4c, differential scanning calorimetry the thermogram for AmB shows a baseline and distinct thermal events. These transitions indicate AmB's has a crystalline nature. The sharp peaks correspond to the melting and decomposition temperatures, indicating thermal stability and unique thermal properties. The lack of significant thermal broadening suggests that it has little interaction with other components in its native state. AmB's thermal profile differs from Ole-Blank's. This profile demonstrates the oleosome carrier system's thermal and structural stability. The thermal behaviour's independence from AmB may be confirmed by a broad endothermic peak, which could signify lipid melting transitions or disruption of the oleosome structure. The OleBlank formulation's thermal peak at 150–175 °C indicates phospholipid bilayer melting (eg, Lipoid S100). Its absence in AmB-loaded Ole1 may indicate successful drug incorporation due to drug–lipid interactions that disrupt crystalline packing.The ole curve shows a thermal profile that combines lipid and oleosome characteristics.[46,72,73] A sharp endothermic peak that differs from Ole-Blank could indicate encapsulation effects or interactions within the oleosome structure. The encapsulation of AmB and other active pharmaceutical ingredients may increase their stability.

Stability Study

Table 4. illustrated the EE%, PS, PDI, and ZP of AmB-Ole during storage for three months at room temperature (25 ± 1 °C), and in the refrigerator (4 ± 1 °C). After storage for three months, the optimized formulae AmB-Ole showed no alterations in their appearance when subjected to various storage conditions. At zero-time, PS was 175±0.78 nm, which non-significantly increased to 175±0.02 and 177±0.91 nm at room temperature by the end of the experiment ($P < 0.05$) which might be attributed to particle fusion during storage. The initial ZP for AmB-Ole was 31±0.43 mV respectively at zero time. ZP non-significantly changed to 30±0.03 and 29±0.21mV respectively at room temperature. Whereas EE% did not significantly decrease from 91±0.63 to 90.9±0.32 and 90.3±0.28. These findings indicated that the optimized formulae AmB-Ole 10 exhibited greater stability at refrigerator temperature, hence maintaining their efficacy for an extended duration during storage.[37,74]

Fabrication of AmB-Ole/MNs

Fabrication of SP/PEG-5000/Chitosan microneedles loading lyophilized Amphotericin-B Oleosomes were made by optimizing polymer matrix composition for mechanical properties, stability, and drug release M1, M2, and M3 SP, PEG-5000, and chitosan concentrations affect MN structure and function. M1 (3% SP, 15% PEG-5000, 10% Chitosan) has the most chitosan and the least SP and PEG-5000 as shown in Table 2. MN's semi-crystalline and robust intermolecular interactions may toughen structures with more chitosan. Low SP brittles flexible MNs. Lots of chitosan may help freeze-dried oleosomes and amphotericin B release drugs. Drug delivery may be delayed by dense matrix. M2 polymer composite: 6% SP, 10% PEG-5000, 15% Chitosan. Chitosan makes SP and PEG-5000 stronger and more

Table 4 The Short-Term Stability Results of Optimized Spanlastics at 4 °C and 25 °C for 3 Months. Mean ± SD (n = 3)

Parameters	AmB-Ole Freshly Prepared	AmB-Ole After 3 Months of Storage at 4 °C	AmB-Ole After 3 Months of Storage at 25 °C
EE (%)	91±0.63	90.9±0.32	90.3±0.28
PS (nm)	175±0.78	175±0.02	177±0.91
PDI	0.33±0.04	0.32±0.01	0.34±0.01
ZP (mV)	31±0.43	30±0.03	29±0.21

Abbreviations: AmB-Ole, Amphotericin -B loaded oleosomes; EE%, entrapment efficiency percent; PS, particle size; PDI, polydispersity index; ZP, zeta potential.

flexible than M1. The efficiency of drug loading optimizing polymer matrix may improve drug loading and oleosome dispersion, controlling release profile. M2 should release faster than M1 but slower than M3 due to its less compact matrix. M3 has the most PS & PEG-5000 and the least chitosan (9%, 5%, 25%). SP and PEG-5000 make microneedles more flexible and penetrate the ocular, reducing ocular breakage. Plasticizing PEG-5000 makes needles. Lower chitosan levels create a porous, hydrophilic matrix that may release AmB and oleosomes faster. Flexible, cohesive SP supports microneedle matrix. Manufacturing with SP (M3) increases mold filling and elasticity. The SP gives MNs shape and flexibility. Biocompatible and biodegradable, it degrades on the ocular. Chitosan stabilizes, antimicrobials, and strengthens MNs. High (M1) concentrations strengthen structure but slow drug release. Applications requiring strong MNs and sustained drug release suit M1. The M2 balances mechanical strength, flexibility, and controlled release. M3 is flexible and speeds up drug delivery, but M1 is durable, for optimal performance, the Multipurpose M2 balances these attributes, and drug-specific microneedles are suggested by systematic polymer ratio variation.[43,75] The crosslinking agent sodium polyacrylate was selected because of its high water absorption capacity, ionic conductivity, and capacity to create robust hydrogel networks. These properties enhance mechanical strength and mucoadhesion. To make microneedles more flexible and less brittle, a plasticizer called PEG 5000 was used. This made them easier to insert into the eye and reduced the risk of mechanical damage.Table 2 shows that Formulation M3 contains the highest concentrations of sodium polyacrylate and PEG-5000, as well as the lowest amount of chitosan. The increased PEG-5000 content acts as a plasticizer, increasing the flexibility of the microneedles and decreasing the risk of breakage during ocular insertion. Sodium polyacrylate helps to create a cohesive, elastic matrix by means of structural integrity. These components taken together provide a safe, minimally invasive ocular delivery system and improve mechanical performance. Though present in lesser levels in M3, chitosan adds antimicrobial action and biocompatibility.

Evaluation of AmB-Ole/MNs Patch

Studies on Drug Content

As shown in Table 5, the drug loading was highest in M3 (95%), followed by M2 (70%), and M1 (54%). M3 has more drugs because its optimized polymer composition improves encapsulation and retention. The high drug content of M3 suggests it can deliver a more concentrated dose of AmB per application, improving therapeutic efficacy. Drug content is crucial to microneedle therapeutic efficacy for ocular infection.M3 exhibited the highest drug loading at 95%, exceeding M1 at 54% and M2 at 70%. The increased chitosan concentration in M3 improves the interaction between the polymer and AmB, resulting in more drug content. M3 is ideal for high-dose AmB administration due to chitosan's positive charge and biocompatibility, which most likely improves drug encapsulation. The lower drug concentrations in M1 and M2 suggest that their polymer compositions may be ineffective in binding or encapsulating AmB. This constraint may limit their therapeutic efficacy, especially in high-dose or extended-release scenarios.[27,76]

Mechanical Characterization

Table 5. compared the length, tip diameter, base diameter, and mechanical resistance under applied forces of three microneedle formulations (M1, M2, and M3). The initial microneedle lengths were 243 µm (M2) to 277 µm (M3), with

Table 5 Physical Characteristics of the Microneedles

MNs	Length (µm)	Tip Diameter (µm)	Base Diameter (µm)	Drug content (%)	Length after Forces Applied per Array(µm)		
					250gm	500gm	1000gm
M1	253 ± 0.21	16 ± 0.04	109 ± 0.56	54	241± 0.41	213 ± 0.23	202 ± 0.76
M2	243± 1.10	19 ± 0.21	102 ± 0.12	70	237 ± 0.11	221 ± 0.05	212 ± 0.50
M3	277± 0.05	12 ± 0.01	105± 0.32	95	275± 0.71	271± 0.41	260± 0.22

Notes: All microneedles contain 400µg of AmB. Each array contains 400 µg of Amphotericin B (AmB). Microneedle height after application of mechanical force (250 g, 500 g, 1000 g per array) reflects their mechanical resistance. A smaller reduction in needle length after force application indicates greater structural integrity and mechanical robustness, which is essential for successful insertion into ocular tissue without bending or breaking.

Abbreviations: MNs, Microneedle; M1, microneedle containing 3%, 15%, and 10% of sodium polyacrylate; PEG5000, and chitosan respectively, M2, microneedle containing 6%, 10%, and 15% of sodium polyacrylate; PEG5000, and chitosan respectively; M3, microneedle containing 9%, 5%, and 25% of sodium polyacrylate; PEG5000, and chitosan respectively.

M3 being the longest. Each formulation's sodium polyacrylate, PEG5000, and chitosan proportions may affect length. With 25% chitosan, M3 held its length under force. M3 retained 94% of its length after 1000 g, compared to 80% for M1 and 87% for M2. Chitosan may increase mechanical strength and dimension stability. The initial microneedle lengths were 243 µm (M2) to 277 µm (M3), with M3 being the longest. Each formulation may have different sodium polyacrylate, PEG5000, and chitosan proportions, explaining this length variation. M3, with the highest chitosan concentration (25%), retained most of its length under force. M3 retained 94% of its length after 1000 g, compared to 80% for M1 and 87% for M2. Chitosan may boost mechanical strength and dimension stability.[77,78]

Tips of microneedles ranged from 12 µm (M3) to 19 µm (M2), with M3 having the sharpest tips. Sharper tips weaken skin penetration. Base diameters were nearly uniform across formulations, ranging from 102 µm (M2) to 109 µm (M1). Because of its mechanical durability and narrow tip diameter, M3 shows promise for invasive ocular drug delivery with minimally invasive procedures. The tip diameter of the microneedles varied between 12 µm (M3) and 19 µm (M2), with the sharpest tips found on M3. Sharper tips require less force to penetrate the ocular. From M2 to M1, base diameters ranged between 102 and 109 µm, indicating a nearly consistent structure. M3's mechanical resilience and small tip diameter make it a promising candidate for minimally invasive drug delivery. Mechanical Strength through force for a microneedle to be useful, it needs to be able to withstand forces during insertion without breaking. To prove its mechanical strength, M3 had the smallest length reduction at 250, 500, and 1000 g. Nevertheless, under the same conditions, M1 exhibited the largest length reduction, indicating that optimization of the formulation is necessary to enhance structural stability. Microneedles that work properly resist forces without distorting as they are inserted. M3 had the least length reduction under 250 g, 500 g, and 1000 g, proving its mechanical strength. In contrast, M1 had the greatest length reduction under the same conditions, indicating the need for formulation optimization to improve structural stability.M3 was the most promising formulation due to its optimal length, sharpness, drug content, and mechanical strength. M3 can ocular delivery of AmB reliably due to these qualities.[25] The M3 formulation exhibited the least deformation, indicating superior mechanical integrity, with a height reduction of 6% under 1000 g. Measuring tip diameter (12–19 µm), base diameter (102–109 µm), and length (243–277 µm), we then computed the aspect ratio. With an ideal aspect ratio of about 2.5, M3 balanced mechanical resilience with penetration.

Characterization of Optimized Microneedle

Scanning Electron Microscopy (SEM)

Figure 5. showed the morphology of M3 microneedles' composition affects their morphology, as shown by SEM images. Sodium polyacrylate, PEG5000, and chitosan are balanced to make microneedles with sharp tips, smooth surfaces, and strong mechanical properties. Ocular drug delivery requires these features for precise, safe, and effective therapy. Sodium polyacrylate crosslinks and stabilizes microneedles, giving them structure. Keeps microneedle tips sharp and defined, as seen in high-magnification SEM images. Prevents fabrication and insertion deformation by increasing mechanical strength. PEG5000 plasticizes the microneedle matrix, making it more moldable. Smooth microneedle surfaces, reducing irregularities. Promotes uniform tip formation for sharpness and flexibility to avoid brittleness. Biocompatible and biodegradable chitosan is M3's main structural material. High concentration (25%) significantly affects microneedle morphology. Provides a sturdy framework to keep microneedles in shape during and after fabrication. Chitosan's adhesive properties make microneedles more mechanically stable, which is essential for ocular insertion. Smooths and uniformizes microneedle surfaces, improving patient comfort. This combination produces sharp, well-defined microneedle tips for ocular tissue penetration. A smooth, uniform surface reduces friction and irritation during application.[79,80]

Fourier Transform Infrared (FTIR) Spectroscopy

The FTIR spectra of BlankMNs and OleMNs represent the sodium polyacrylate-PEG/Chi microneedles (MNs) without and with oleosomes containing AmB as shown in Figure 4b. The Blank-MNs spectrum shows characteristic peaks of the sodium polyacrylate-PEG/Chi matrix. The strong peak near 1550 cm^{-1} corresponds to asymmetric stretching of the carboxylate group (COO^-) of sodium polyacrylate, while a peak near 1400 cm^{-1} arises from symmetric COO^- stretching. Peaks around 3300–3400 cm^{-1} indicate N–H and O–H stretching vibrations, likely from chitosan and PEG-5000. C–H stretching vibrations are observed at 2920 cm^{-1} and 2850 cm^{-1}, reflecting the aliphatic components of PEG

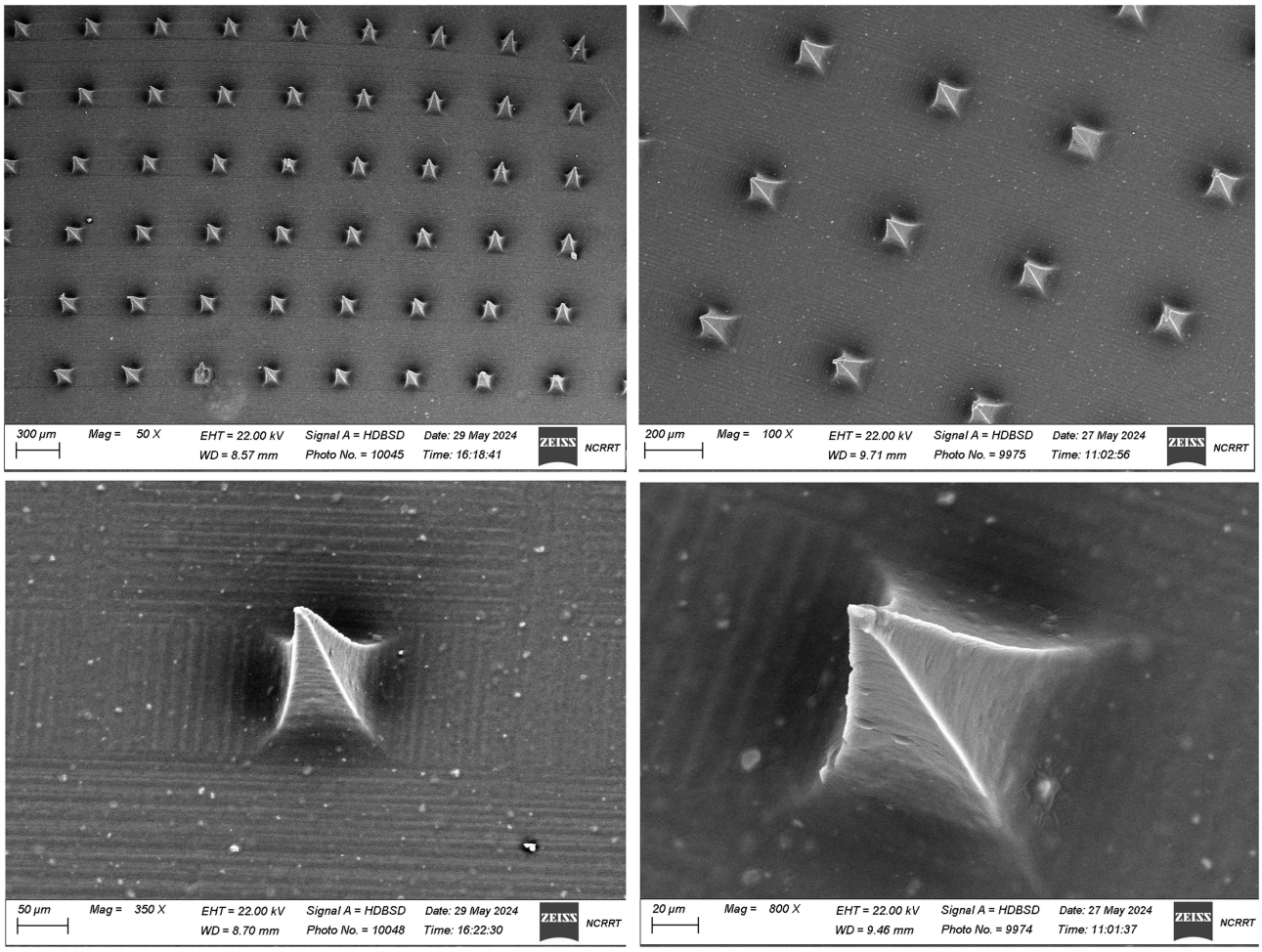

Figure 5 Scanning electron microscopy of optimized SP-PEG/Chi-Microneedle loading freeze-dried Amphotericin -B -loaded Oleosomes (M3).

and chitosan. The OleMNs spectrum shows features of both the MNs matrix and the oleosomes with Amphotericin B. Peaks around 2920 cm^{-1} and 2850 cm^{-1} are more pronounced, reflecting the lipid content of the incorporated oleosomes. The appearance of peaks at 1650 cm^{-1} and 1550 cm^{-1} confirms the presence of Amphotericin B in the oleosomes within the MNs. The broadening and increased intensity of the O–H/N–H stretching region (3300–3400 cm^{-1}) suggest interactions between the oleosome's lipids and the MNs matrix, potentially through hydrogen bonding.[76,81] The FTIR spectra confirms the successful incorporation of Amphotericin B into oleosomes (Ole10) and their further integration into the microneedle system (OleMNs). The distinct molecular signatures of Amphotericin B, oleosomes, and the MNs matrix are preserved, with shifts and broadenings indicating interactions between these components.[24]

Differential Scanning Calorimetry (DSC)

Figure 4c. show the thermal profile of Blank-MNs (sodium polyacrylate-PEG/chitosan-based microneedles) that are not loaded with oleosomes, the DSC curve shows subtle endothermic and exothermic transitions, which could correspond to polymer thermal properties like glass transition or decomposition temperatures. Since there are not any clear peaks, it means that there is not any significant crystalline material present. This means that the microneedles are most likely made of an amorphous polymer.[68,82] Ole-MNs display the heat behaviour of microneedles filled with oleosomes that surround AmB. When compared to Blank-MNs, the changes in peak position or thermal transitions show that oleosomes are present in the matrix. Thermal events indicate an interaction between the microneedle matrix and the oleosome components, which most likely contributes to the increased stability of the encapsulated AmB. This interaction may delay AmB's thermal decomposition while improving its overall thermal properties. The DSC data demonstrates the

distinct thermal behaviors of the components and formulations. AmB has distinct thermal properties, with well-defined transitions. Oleosomes (Ole) improve stability, whereas Blank-MNs show typical polymer behavior. The microneedle system's endothermic peak at 150 °C in BlankMNs is due to PEG-5000 and sodium polyacrylate melting. The disappearance of this peak in OleMNs suggests a homogeneous dispersion or interaction between AmB-Ole and the polymeric matrix, resulting in altered thermal behavior. Microneedles containing oleosomes encapsulating AmB (MNs) show a synergistic effect, with improved thermal stability indicating effective formulation integration.

Drug Release Studies

In vitro Drug Release Study

Figure 6a. showed the In-vitro release of AmB solution, AmB-Ole, and AmB-Ole/MNs, the AmB Solution has a rapid release, reaching approximately 95% within 8 hours. This rapid release has poor sustained release characteristics because the drug diffuses quickly into the surrounding medium without any controlled mechanism. AmB-Ole Within 24 hours, approximately 80% of the solution is released, after which it stabilizes, resulting in a more gradual release. After 8 hours, AmB-Ole releases approximately 60%, 37% less than the solution's release rate. The free AmB solution exhibited the fastest release profile due to its immediate availability in the dissolution medium. In contrast, the AmB-Ole/MNs formulation showed the slowest release rate. This can be attributed to the dual encapsulation system, where AmB is first

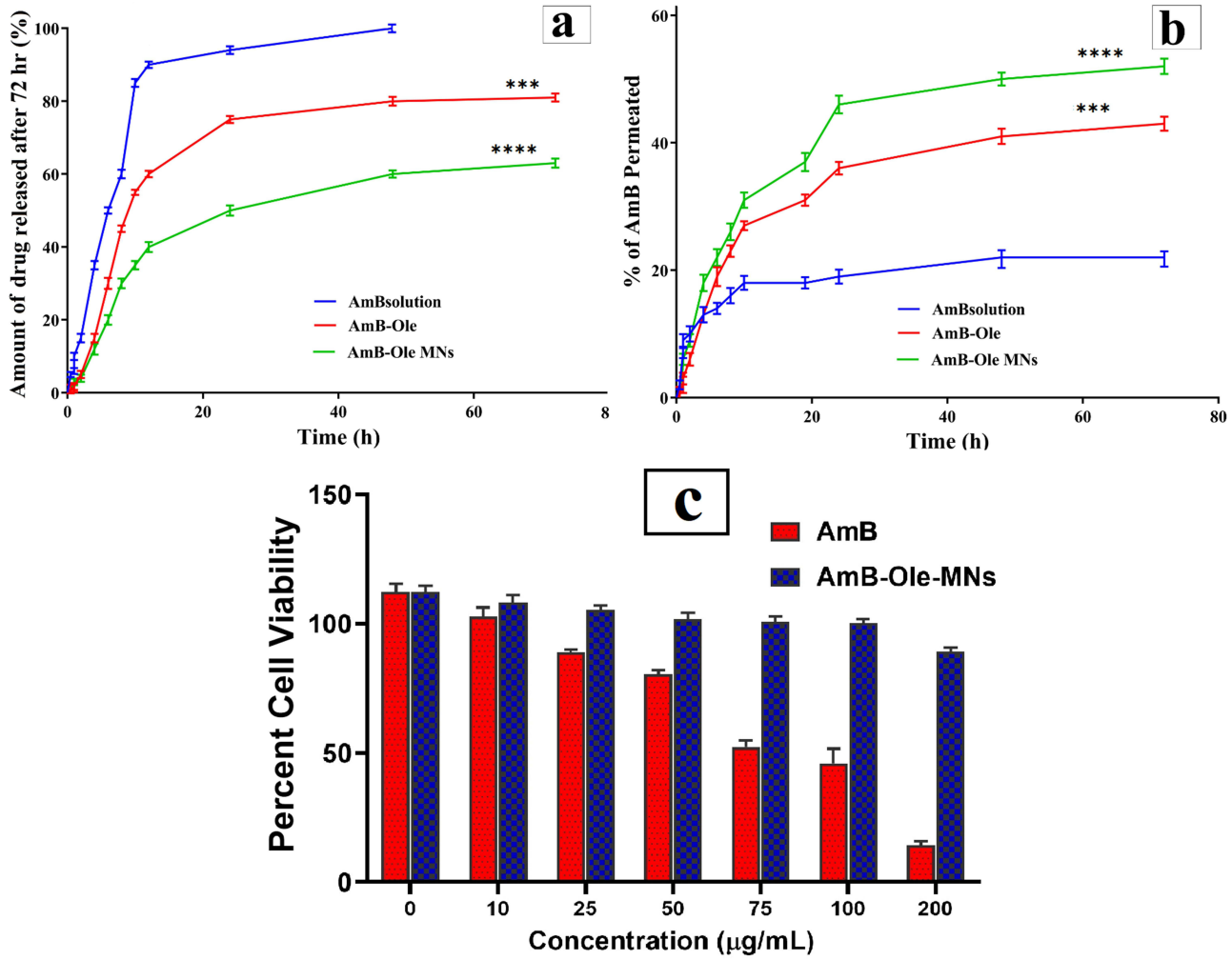

Figure 6 (**a**) In vitro drug release study, (**b**) Ex vivo permeation studies for AmB solution, AmB-Oleo, AmB-Ole MNs respectively, and (**c**) Effect of AmB and AmB-Ole-MNs on HaCaT cell viability. Cell viability of 100% corresponds with untreated cell MTT average reduction value.
Note: Data are presented as Mean ± SD: ***P < 0.001, and ****P < 0.0001.
Abbreviations: AmB, Amphotericin-B solution; AmB-Ole-MNs, Optimized oleosomes loaded amphotericin-B microneedle.

https://doi.org/10.2147/IJN.S514798

entrapped within oleosomes and then embedded in the hydrogel microneedle matrix. The release is therefore controlled by both the diffusion from oleosomes and the gradual hydration and erosion of the microneedle structure, resulting in sustained drug delivery over time. Oleosomes regulate release using their lipid bilayer architecture, which serves as a reservoir and slows drug diffusion. Reduces the initial burst release by approximately 15%, resulting in a more consistent drug release profile. AmB-Ole MNs have the slowest release kinetics, releasing approximately 40% within 24 hours and 65% after 72 hours. After 8 hours, approximately 30% of the drug has been released, which is 68% slower than the solution and 50% slower than AmB-Ole. Microneedles act as an additional controlled-release matrix, trapping the drug and extending its release time. At 72 hours, it demonstrates approximately 30% more sustained release than AmB-Ole, making it the ideal candidate for long-term drug delivery. Because of their sustained release, AmB-Ole MNs can reduce dosing frequency while maintaining therapeutic concentrations. This reduces patient discomfort and improves compliance when treating fungal keratitis.[70,83] The dual encapsulation strategy and hydrogel microneedle matrix properties are responsible for the AmB-Ole/MNs' sustained release profile. After administration, the microneedles absorb ocular fluid and swell, creating a hydrogel barrier that slows drug diffusion. Amphotericin B must first diffuse from oleosomes and then through the polymer matrix, resulting in sequential diffusion steps. Additionally, the semi-crosslinked network of sodium polyacrylate and chitosan slows matrix erosion and water penetration, further extending the release period. This controlled mechanism is beneficial for maintaining prolonged therapeutic levels on the ocular surface.

Ex vivo Permeation Studies

Figure 6b. shown the AmB Solution demonstrated minimal permeation, attaining approximately 20% penetration at 24 hours and maintaining this level until the conclusion of the experiment. The suboptimal efficacy is ascribed to the elevated molecular weight and hydrophilicity of amphotericin B, which restricts its penetration through the corneal epithelium. The AmB solution does not achieve therapeutic concentrations in the corneal layers, rendering it ineffective for deep ocular infections, though it may be appropriate for superficial infections or as an initial treatment. Ex vivo permeation studies demonstrated that the AmB-Ole MNs enhanced drug penetration by approximately 90% compared to the AmB solution and 25% compared to the AmB-Ole formulation. These differences were statistically significant ($p < 0.05$), as confirmed by one-way ANOVA followed by Tukey's test. These findings suggest that AmB-Ole MNs are the most effective formulation for achieving therapeutic concentrations of Amphotericin B in corneal tissues. This enhancement results from oleosomes augmenting AmB's lipophilicity and promoting drug translocation across the corneal epithelium by emulating natural lipids.[65,84] The formulation provides therapeutic concentrations to deeper corneal layers, rendering it appropriate for moderate ocular fungal infections or for patients who cannot utilize microneedle-based therapies. The AmB-Ole MNs had the best permeation, with a penetration of about 60% after 24 hours (which is 30% higher than AmB-Ole and 100% higher than the solution) and about 70% after 80 hours. By puncturing the corneal barrier and creating short-lived microchannels, microneedles enhance delivery by allowing AmB to diffuse directly into deeper tissues. Incorporating oleosomes improves both drug stability and controlled release. AmB-Ole MNs are ideal for serious systemic infections such as fungal keratitis due to their long-acting drug release, enhanced penetration, and prolonged therapeutic effect. The findings of the ex vivo study indicate that AmB-Ole MNs are the best formulation for therapeutic concentrations of amphotericin B to be applied to the cornea. Although it is not as effective as the microneedle-based system, AmB-Ole is an excellent alternative to the conventional solution.Liposomes, solid lipid nanoparticles (SLNs), and nanostructured lipid carriers (NLCs) are among the nanocarriers being studied for the delivery of Amphotericin B; however, these methods have their limitations when it comes to ocular applications. Liposomes are biocompatible, but they can be unstable and drug leakage can occur. Solid lipid nanoparticles (SLNs) and nanostructured lipid carriers (NLCs) exhibit enhanced stability; nonetheless, they present challenges related to low drug loading capacity and restricted penetration through ocular barriers.Mechanically inserting microneedles into the corneal epithelium creates transient microchannels, which increase corneal penetration with AmB-Ole/MNs. Encapsulated drugs can diffuse directly into deeper ocular layers through these microchannels, bypassing tight junctions. Chitosan, a positively charged polymer, may also improve adhesion and corneal surface residence time by strengthening electrostatic interactions with negatively charged ocular mucins. Drug permeation in ex vivo studies is greatly improved by this dual mechanism.

Cytotoxicity and Biocompatibility

Figure 6c. shown the results clearly show that AmB-Ole-MNs are more biocompatible than free AmB. Amphotericin B, a potent antifungal agent, is known for its dose-dependent cytotoxicity caused by its direct interaction with cholesterol-rich cell membranes, which results in membrane disruption and cell death. The current study found that AmB was toxic at concentrations of ≥50 µg/mL. The AmB-Ole-MNs formulation had low cytotoxicity, even at higher concentrations (200 µg/mL). This can be attributed to the micellar structure, in which oleic acid MNs AmB and regulate its release.[58,85,86] There is a big difference in how well cells can live between AmB and AmB-Ole-MNs. This shows that MNs formulations can work around the issues Caused by Free AmB. It looks like micellar systems could help get drugs to more people because they make drugs more stable and easier to dissolve while hurting cells less. The research demonstrated that AmB-Ole-MNs markedly diminished the cytotoxicity of AmB solution on HaCaT cells. The free AmB diminished cell viability in a dose-dependent fashion, whereas the micellar formulation preserved high cell viability across all tested concentrations. These findings highlight the remarkable biocompatibility of AmB-Ole-MNs and their promising clinical potential, particularly in reducing the harmful effects of AmB.[87]

Antifungal Activity

In Figure 7, and Table 6 ole-blank inhibited *C. albicans* with a ZOI of 17 ± 0.45 mm, MIC of 125 ± 0.01 µg/mL, and MBC of 1000 ± 2.21 µg/mL The oleosome carrier is antifungal because oleic acid breaks fungi cell membranes. AMB

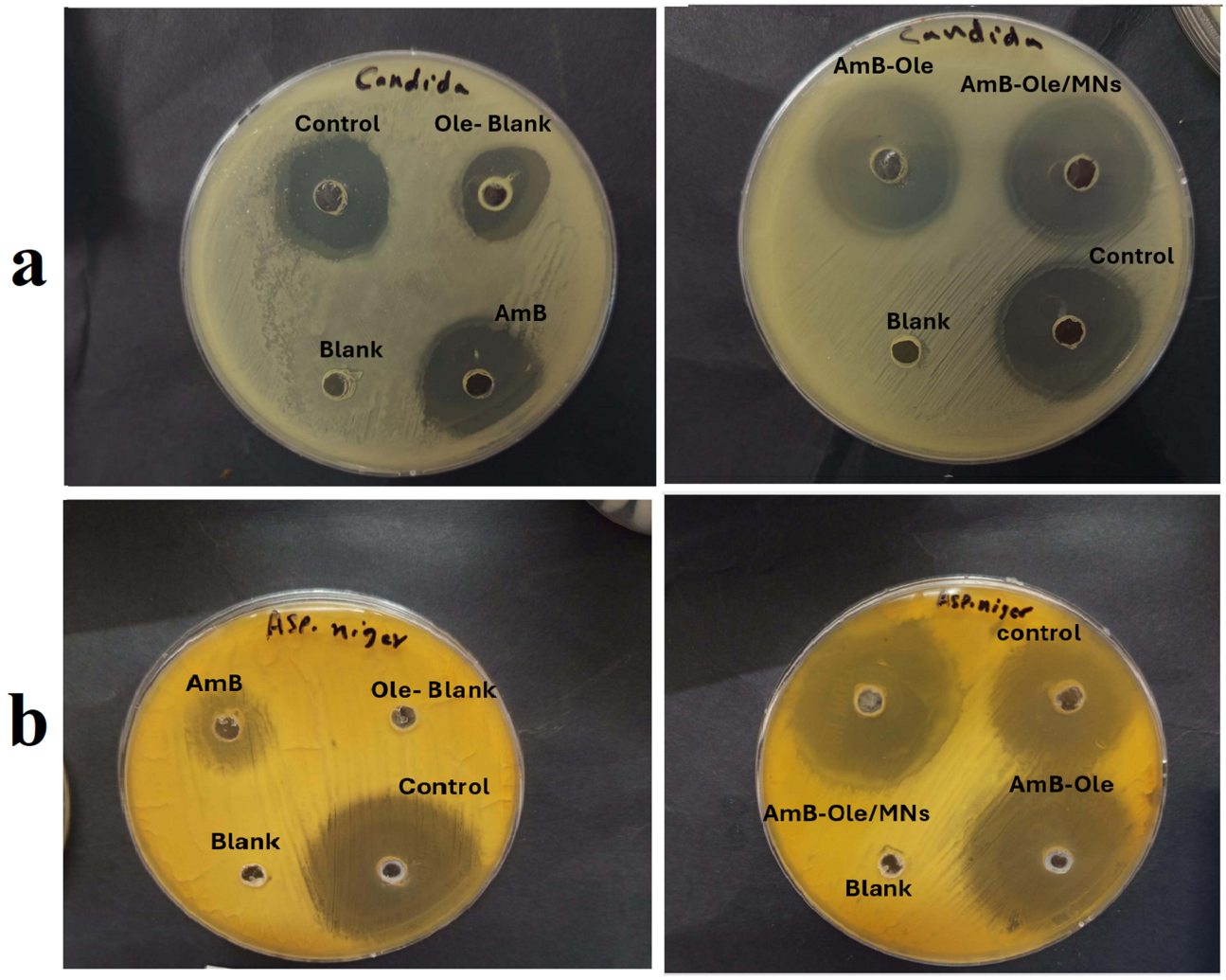

Figure 7 In-vitro anti-fungal activity (**a**) against *Candida albicans*, and (**b**) *Aspergillus Niger* for AmB solution, Ole-Blank, AmB-Ole, and AmB-Ole/MNs as compared to Fluconazole as control using agar disc diffusion method.

https://doi.org/10.2147/IJN.S514798

Table 6 In-vitro anti-Fungal Susceptibility of the Ole-Blank, Fluconazole (Control), AmB, AmB-Ole, AmB-Ole/MNs (n = 3 ± SD)

Fungal Strains	Item Under Test	The Diameter of Zone in (mm)(Mean±SD)	MIC (μg/mL) (Mean±SD)	MBC (μg/mL) (Mean±SD)
Candida albicans (ATCC 10221)	Ole-blank	17±0.45	125.00±0.01	1000.00±2.21
	Control	25±0.25	63.50±0.21	125.00±0.23
	AmB	23±17	62.52±0.44	125.00±0.23
	AmB-Ole	25±0.21	31.25±0.44	125.00±0.81
	AmB-Ole/MNs	27±0.42	17.81±0.65	62.50±0.57
Aspergillus niger (ATCC 16888)	Ole-blank	9±0.11	NA	NA
	Control	25±0.71	320.00±0.35	1000±0.71
	AmB	17±11	250.00±0.43	1000±9.12
	AmB-Ole	25±02	31.25±0.51	125±0.72
	AmB-Ole/MNs	32±13	15.62±0.35	125±135

Note: MBC represents the lowest concentration required for 99.9% fungal killing.
Abbreviations: Ole-blank, oleosomes formula without drug; AmB-Ole, Amphotericin-B-Oleosomes; AmB-Ole/MNs, Amphotericin-B-Oleosomes Microneedle.

binds to ergosterol, causing fungal membrane pores and cell death. The ZOI, MIC, and MBC of the AmB solution were 23 ± 17 mm, 62.52 ± 0.44 μg/mL, and 125 ± 0.23 μg/ Low bioavailability and solubility reduce efficacy. AmB-Ole showed enhanced antifungal activity, with a ZOI of 25 ± 0.21 mm, MIC of 31.25 ± 0.44 μg/mL, and MBC of 125 ± 0.81 μg. AmB's solubility, stability, and oleosome targeting benefit fungal biofilms and cell membranes. AmB-Ole/MNs had the highest antifungal activity with a ZOI of 27 ± 0.42 mm, MIC of 17.81 ± 0.65 μg/mL, and MBC of 62.5 ± 0.57 μg/mL Oleosomes and microneedles improve performance. Oleosomes stabilize drugs, and microneedles clean corneal biofilms. Oleosome blanks had low antifungal activity (9 ± 0.11 mm ZOI) against A. niger, with no MIC or MBC. The more resistant A. niger strain may survive oleic acid. In free AmB, moderate activity was observed with a ZOI of 17 ± 11 mm, MIC of 250 ± 0.43 μg/mL, and MBC of 1000 ± 0.71 μg for penetration and solubility, AmB kills A. niger but not biofilms or resistant strains, AmB-Ole demonstrated enhanced antifungal efficacy with a ZOI of 25 ± 0.02 mm, MIC of 31.25 ± 0.51 μg/mL, and MBC of 125 ± 0.72 μg/mL Fungal cell walls and membranes interact better with oleosomes. AmB-Ole/MNs using the microneedle formulation, A. niger was inhibited with a ZOI of 32 ± 13 mm, MIC of 15.62 ± 0.35 μg/mL, and MBC of 125 ± 1.35 μg/mL. The oleosome transports and stabilizes drugs while the microneedle system penetrates biofilms and fungal structures. AmB-Ole/MNs were more antifungal than AmB. Oleosome stability, bioavailability, and solubility improve drug-fungal membrane interactions. Microneedles penetrate tissue and break biofilms, increasing effectiveness. Most effective against *C. albicans* and *A. niger* were AmB-Ole/MNs with the highest ZOI, lowest MIC, and lowest MBC. Antifungal and drug delivery are made easier by microneedles and oleosomes. Oleosome blank inhibited *C. albicans* but not *A. niger*. AmB may work better than oleic acid, which disrupts fungal membranes. All formulations' MIC and MBC values showed *C. albicans* was less resistant than *A. niger*. As *A. niger* performed worse than AmB-Ole/MNs, they may treat resistant fungal infections. AmB-Ole/MNs target more fungi and have lower MIC/MBC than free AmB. Oleosomes and microneedles improve solubility, biofilm resistance, and penetration, making them promising *C.albicans* and *A. niger* keratitis treatments. Despite the corneal barrier and fungal biofilms, this dual system penetrates. Transient corneal microchannels created by microneedles reduce dosing frequency and direct drug diffusion to the infection site. Sustainable drug release from microneedles reduces application frequency and improves patient adherence. Chitosan, a biocompatible antifungal, works better and has fewer systemic side effects than high-dose antifungals. These qualities may make AmB-Ole/MNs a good fungal keratitis treatment. AmB-Ole/MNs may be a better FK treatment because it works better, patients take it less often, and they follow their treatment plans.[6,29] The improved antifungal activity of AmB-Ole/MNs, as demonstrated by lower MIC and MBC values and larger zones of inhibition, is most likely due to a combination of factors. First, the oleosome formulation enhances AmB's apparent solubility and dispersion, increasing its bioavailability. Second, oleosomes' amphiphilic structure may make them easier to integrate into fungal cell membranes. Last but not least, the microneedle system allows for direct drug deposition outside of

surface biofilms, resulting in more thorough tissue penetration and effective fungal structure disruption. These mechanisms work together to increase the antifungal efficacy of the AmB-Ole/MNs system.

Effect of the Optimized Formulas on the Antibiofilm Activity

The AmB-Ole/MNs demonstrated the most significant anti-biofilm activity against *C.albicans*, achieving 92.71% at 75% MBC, 88.66% at 50% MBC, and 79.06% at 25% MBC. The outstanding performance is ascribed to the oleosome system, which improves drug solubility, stability, and biofilm penetration. AmB's activity was marginally reduced, with 89.69%, 85.97%, and 70.83% inhibition at 75%, 50%, and 25% MBC, respectively. Although AmB is effective against biofilms, its efficacy is limited by low solubility and penetration into biofilms.AmB-Ole demonstrated moderate anti-biofilm activity (87.05%, 82.92%, and 68.48%), most likely due to oleic acid's inherent antifungal properties, which disrupt fungal cell membranes as shown in Figure 8a and b. The ole blank exhibited the lowest anti-biofilm activity, with percentages of 78.03%, 59.52%, and 32.72%. The observed diminished efficacy may be attributed to the biofilm matrix's decreased penetration and slower drug release at lower concentrations. AmB-Ole/MNs exhibited substantial anti-biofilm activity against *A. niger*, with inhibition of 91.50% at 75% of MBC, 88.16% at 50%, and 79.89% at 25%. The oleosome formulation significantly improves drug delivery, allowing for more substantial disruption of the biofilm structure. AmB solution's potent antifungal properties were confirmed by its high activity (89.83%, 82.11%, and 61.02%). Nonetheless, the results were slightly lower than those of AmB-Ole, highlighting the benefits of oleosomes in increasing drug efficacy. AmB-Ole showed significant activity (85.59%, 76.43%, and 43.62%), indicating that oleosomes have antifungal and biofilm-disruptive properties due to their oleic acid content.[58,88,89] The ole blank exhibited the lowest anti-biofilm activity at 70.56%, followed by values of 63.38% and 27.46%, respectively. This indicates that microneedles enhance drug penetration into tissues; however, their effectiveness in addressing biofilms is limited. The application of AmB-Ole/MNs markedly enhances anti-biofilm efficacy against *A. niger* and *C. albicans*. Oleosomes and microneedles demonstrate enhanced efficacy in dissolving and disrupting biofilms, thereby improving drug solubility, stability, and targeted delivery. Although this study focused on *Candida albicans* and *Aspergillus niger, Fusarium* species are responsible for the majority of fungal keratitis worldwide. Future studies will use animal models to broaden the application of AmB-Ole/MNs in *Fusarium*-induced keratitis. Natamycin and voriconazole are first-line treatments for fungal keratitis, but resistance, poor corneal penetration, and treatment failures continue. In azole-resistant or *Candida*-related infections, amphotericin B is essential despite its toxicity and solubility. A promising adjunct or alternative to existing antifungal treatments, our microneedle-based delivery system improves AmB penetration and tolerability.

In vivo Studies

Eye Irritation Test (Draize Test)

In-vivo testing data in Figure 9a show no evidence of inflammation or corneal, conjunctival, or iris injury. The edema of the conjunctiva and drainage were always graded zero. At all observations, the scores for iris hyperemia and corneal opacity were zero. As a consequence of the absence of *in-vivo* irritating effects, the AmB-Ole and AmB-Ole/MNs can be of therapeutic interest.

In-vivo Antifungal Activity of AmB Formulations (Susceptibility Test)

Figure 9b. Shown *C.albicans* was utilized as the test organism for susceptibility testing, the percentage of growth inhibition of *C. albicans* was correlated with the duration of the drug's presence on the ocular surface after topical application. The inhibition percentage, as indicated by the area under the curve, adhered to the subsequent hierarchy: AmB-Ole/MNs > AmB-Ole > AmB solution. The AmB-Ole/MNs formulation effectively sustained antifungal activity for an extended duration compared to the AmB-Ole, and AmB-Ole solution. The microneedle enhanced the retention of the Amphotericin-loaded oleosomes on the ocular surface, attributable to the bioadhesive properties of chitosan in microneedles. The microneedle formulation may serve as a viable alternative to traditional eye drops due to their prolonged residence time and sustained efficacy.

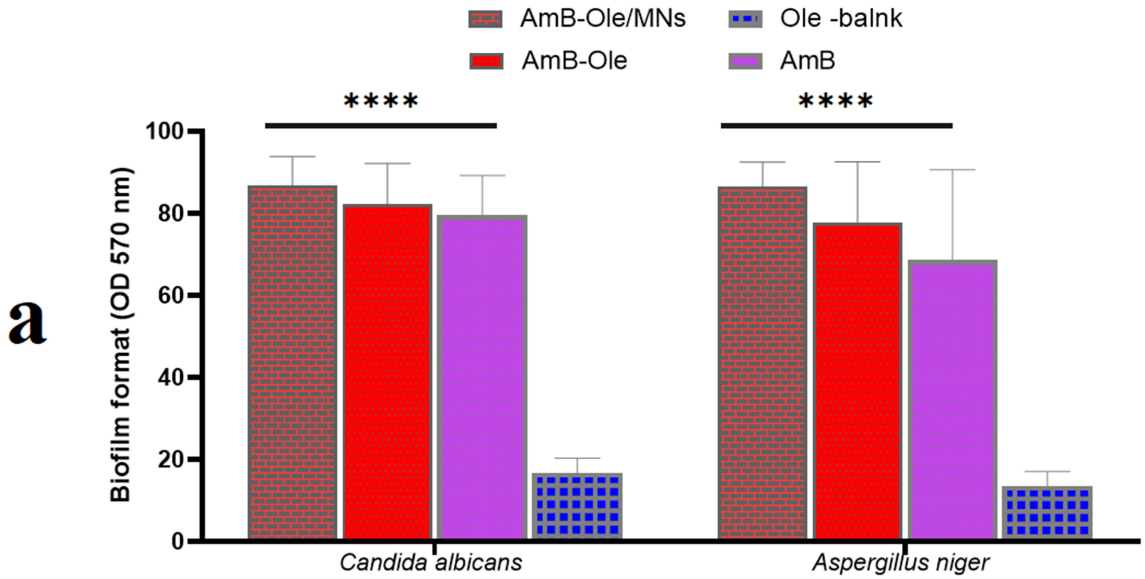

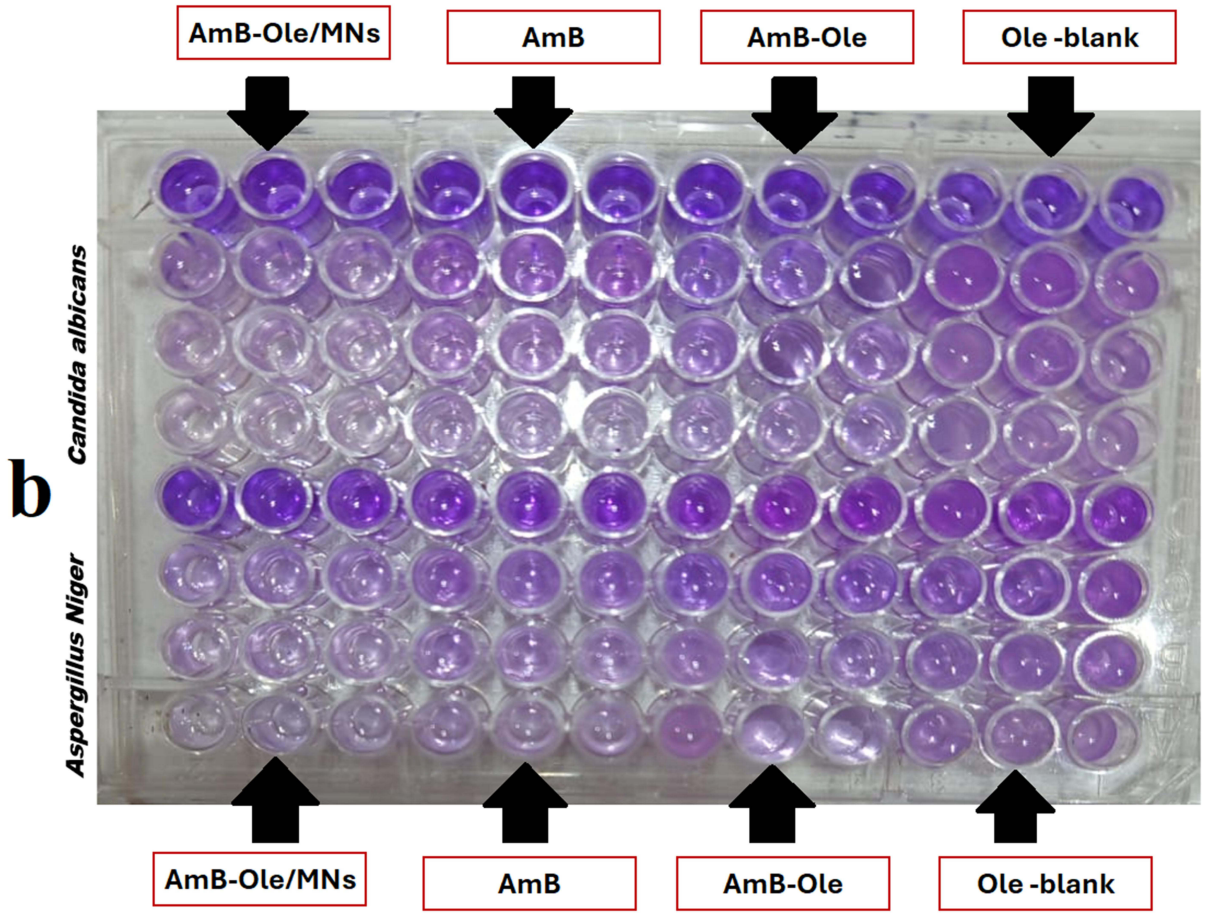

Figure 8 (**a**). Antibiofilm reduction effect of *Candida albicans*, and *Aspergillus niger* (**b**). Crystals violet assay to assess antibiofilm activity of AmB, Ole blank without AmB, AmB-Ole, and AmB-Ole/MNs.
Note: Data are presented as Mean ± SD: ****P < 0.0001.

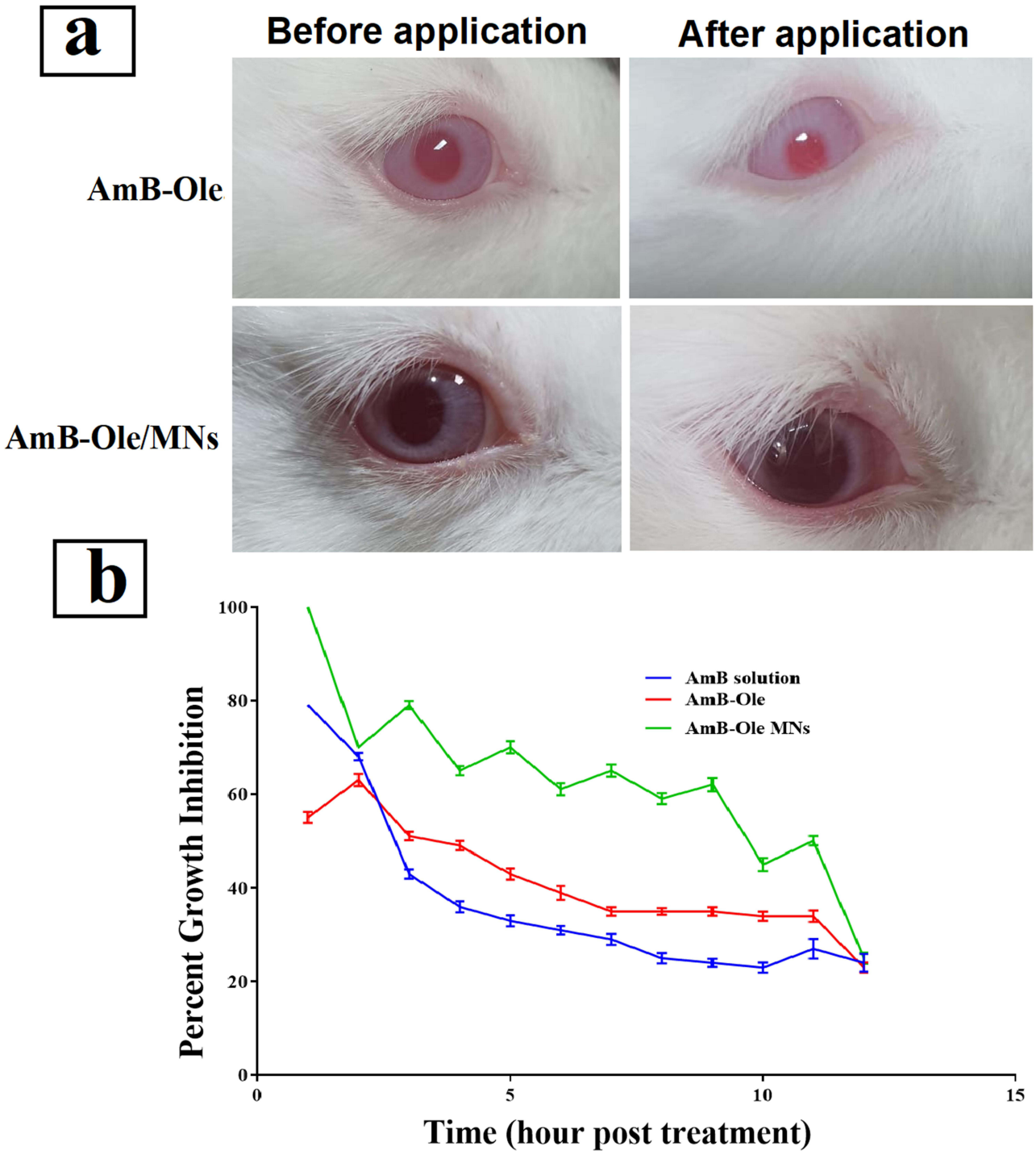

Figure 9 (**a**).Examination of possible ocular irritation following the application of the AmB-Ole and AmB-Ole/MNs formulation, and (**b**)Percentage inhibition of *Candida albicans* growth produced by AmB-Ole, and AmB-Ole/MNs, in the external eye tissues of albino rabbits.

Assessment of Inflammatory Biomarkers

Figure 10. The serum samples were tested for inflammatory biomarkers (NLRP3, IL-6, TNF-α, IL-1β, and TLR4) to assess the response to AmB and its optimized formulations, such as AmB-Ole and AmB-Ole/MNs. These findings revealed that the untreated group had significantly higher levels of all biomarkers compared to the healthy group, indicating a strong inflammatory response caused by infection or disease progression. The AmB solution group exhibited

https://doi.org/10.2147/IJN.S514798

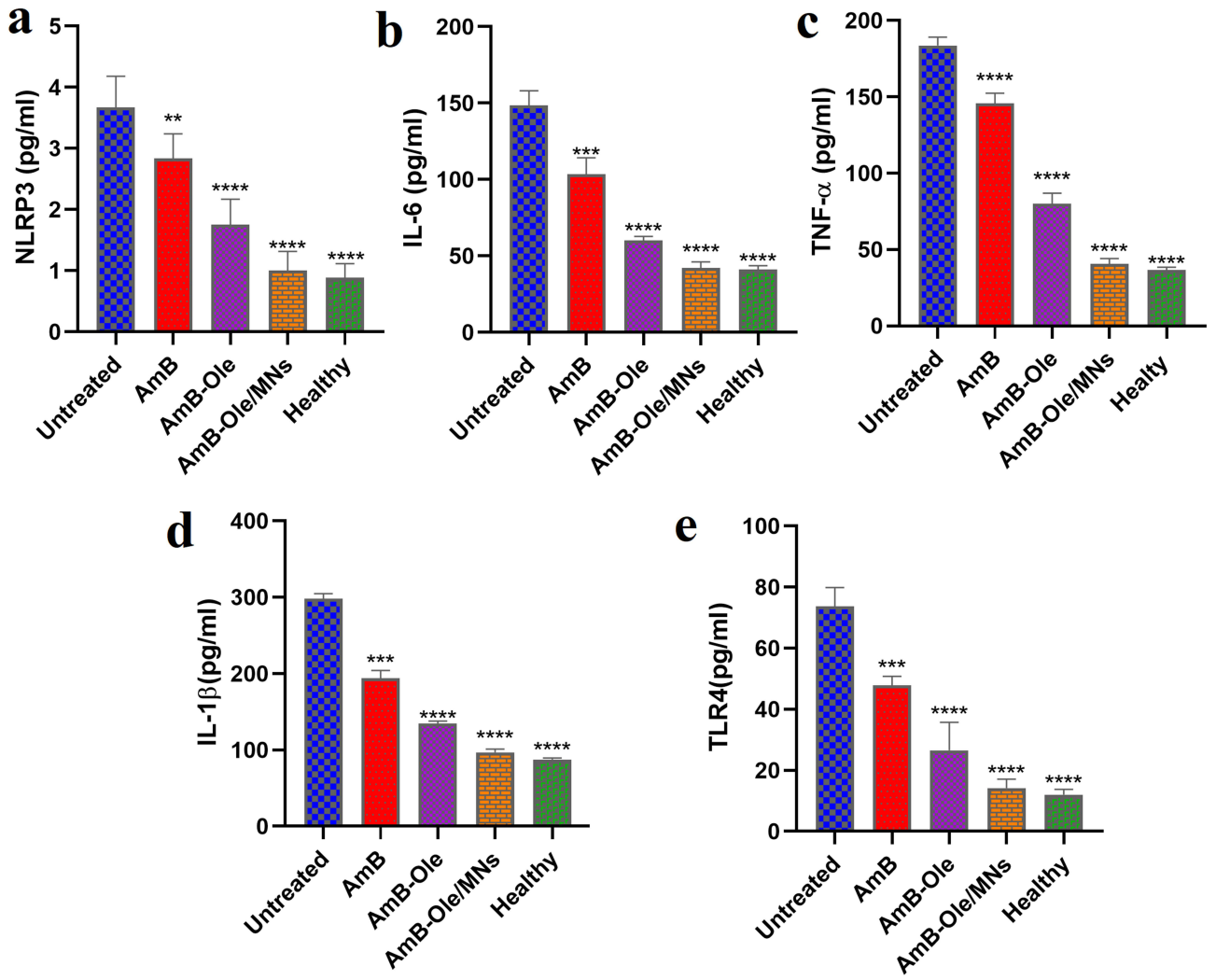

Figure 10 Anti-inflammatory effect of different experimental groups on inflammation (NLRP3 level(**a**), IL-6(**b**), TNF-α(**c**), IL-1β(**d**), and TLR4(**e**)).
Note: Data are presented as Mean± SD (n=6): ****P < 0.0001, ***P < 0.001, and **P < 0.01.
Abbreviations: AmB, Amphotericin-B solution; AmB-Ole-MNs, Optimized oleosomes loaded with amphotericin-B microneedle.

a significant downregulation of NLRP3, IL-6, TNF-α, IL-1β, and TLR4 protein levels compared to the untreated group, indicating that free AmB may partially mitigate inflammation via its antifungal properties.[90] The levels of all inflammatory biomarkers dropped significantly when the AmB-Ole and AmB-Ole/MNs were used compared to the untreated group. These levels were getting closer to those seen in the healthy group in AmB-Ole/MNs in all measured inflammatory biomarkers. The amounts of NLRP3 in the AmB-Ole and AmB-Ole/MNs groups were significantly downregulated compared to those in the untreated group, which means that the inflammasome activation was effectively reduced.[32,52] The optimized formulations had much lower levels of IL-6 and TNF-α compared to the AmB solution group, showing that they were more effective in reducing inflammation. The microneedle formulation (AmB-Ole/MNs) exhibited consistently reduced biomarker levels relative to AmB-Ole, presumably owing to superior drug delivery, enhanced penetration, and prolonged release properties.IL-1β levels, closely associated with NLRP3 inflammasome activation, were markedly diminished in the AmB-Oleosomes and AmB-Ole/MNs groups compared to those in untreated group, thereby underscoring the effectiveness of these formulations in modulating inflammation.[91,92] The healthy group consistently demonstrated the lowest levels of all biomarkers, functioning as a baseline control for comparison. The optimized formulations, especially AmB-Ole and AmB-Ole/MNs, notably reduced the inflammatory response in comparison to free AmB. The decrease in inflammatory levels indicates that these formulations effectively reduce

inflammation and may also mitigate the cytotoxic effects linked to free AmB.The AmB-Ole/MNs group showed significantly lower levels of NLRP3, IL-6, and TNF-α compared to the free AmB group, likely due to the drug's localized and sustained delivery at the infection site. Microneedle-assisted administration allows for direct corneal deposition of AmB, which improves fungal clearance while limiting systemic absorption. This reduces the systemic recruitment of inflammatory mediators while minimizing drug-related toxicity. Furthermore, the controlled release from the hydrogel matrix may also suppress local immune activation, resulting in an overall anti-inflammatory effect. The

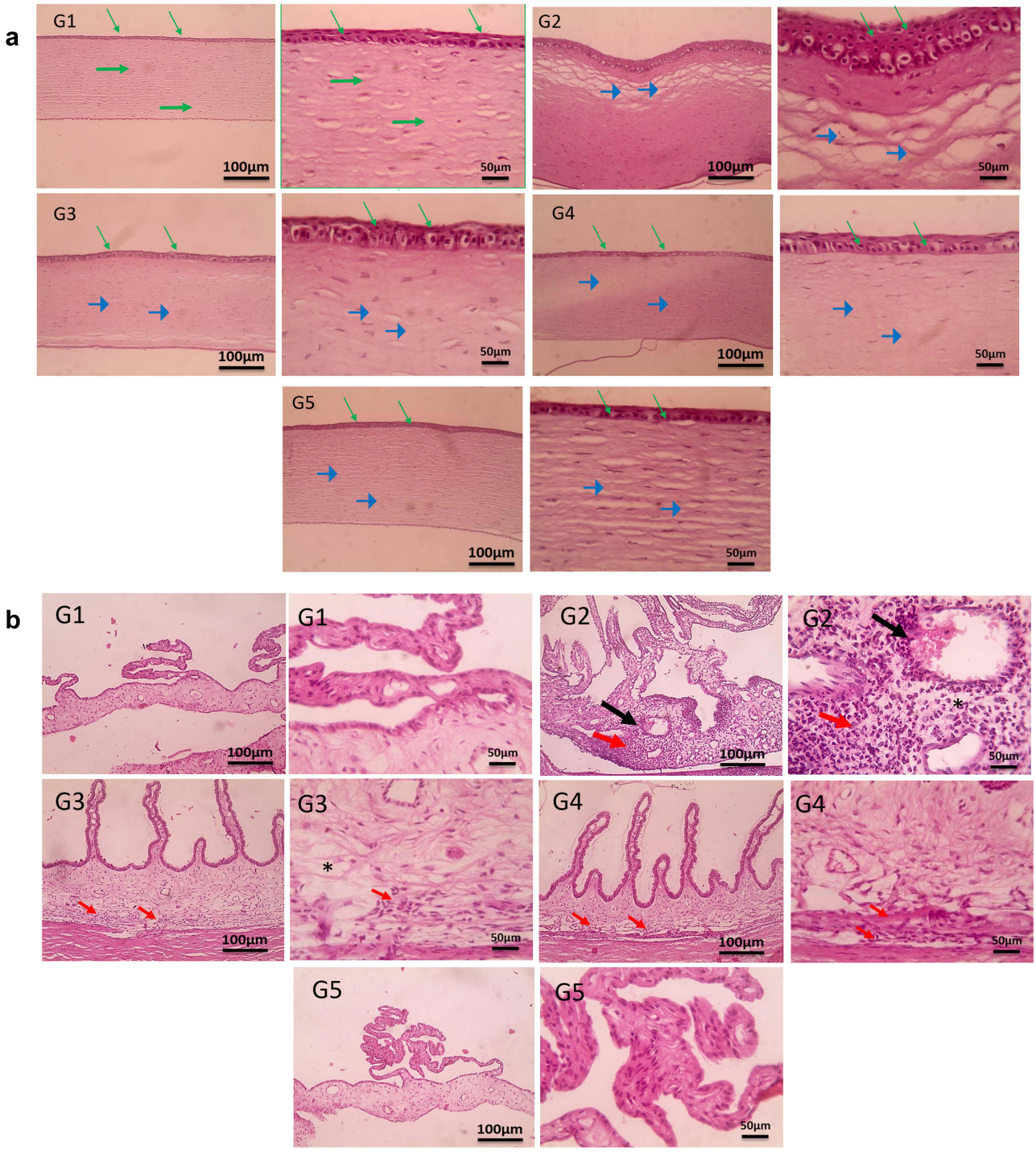

Figure 11 Continued.

https://doi.org/10.2147/IJN.S514798

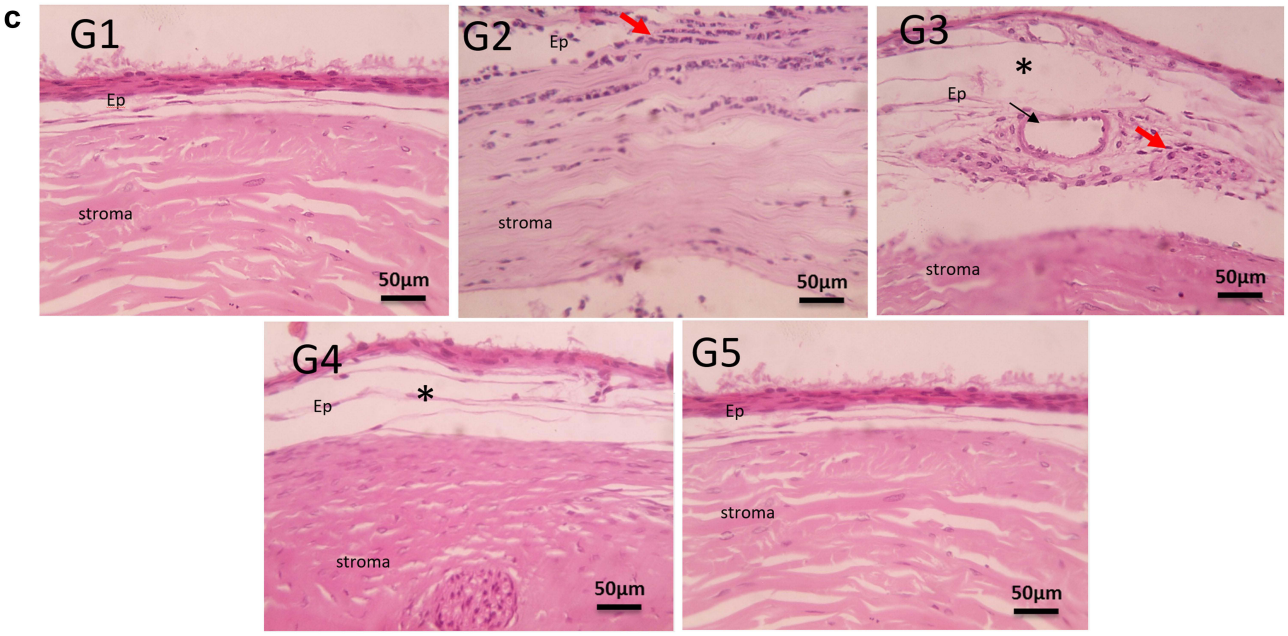

Figure 11 A Histological Examination of Ocular Tissues in Control, Diseased, and Treated Rabbit Eyes (G1–G5): (**a**) Corneal sections from the healthy control group (G1) show normal epithelial and stromal structure. Infected untreated corneas (G2) display severe epithelial vacuolation and stromal edema. Treatment with Amphotericin B solution (G3) reduces epithelial thickness and vacuolation with partial stromal recovery. Optimized Amphotericin B-oleogel treatment (G4) further improves epithelial morphology and stromal integrity. Complete histological restoration is observed in the Amphotericin B-oleogel microneedle-treated group (G5). (**b**) Ciliary body sections from G1 appear normal, while G2 exhibits intense leukocytic infiltration, edema, and vascular congestion. G3 and G4 show progressive reduction in inflammation, with G5 returning to normal histology. (**c**) Scleral sections reveal normal episcleral and stromal architecture in G1. G2 displays leukocytic infiltration and disrupted collagen organization. G3 and G4 show reduced inflammation and vascularization, with G5 demonstrating restored normal scleral and episcleral structure. (Staining: H&E; Magnifications: X100, bar 100 μm; inserts X400, bar 50 μm).

microneedle formulation works effectively, which means it delivers drugs more effectively and offers a promising alternative for better therapeutic outcomes. Furthermore, the results showed that AmB-Ole and AmB-Ole/MNs may be safer and more effective ways to treat inflammatory conditions, similar to the previous reports.[64]

Histological Examination

As shown in Figure 11a, histological examination of the cornea in Group 5 (AmB-Oleosome Microneedles) had a fully restored epithelial layer and an intact stroma, demonstrating a preserved normal histological structure. This result indicates that Group 5 produced the best outcome, leading to a full recovery. In Group 4 (AmB-Oleosomes) the cornea in this group showed significantly less vacuolation and a significantly thinner epithelial layer, but the stroma stayed normal. In group 3 (Amphotericin-B solution), the cornea exhibited reduced thickness of the epithelial layer and diminished vacuolation within the epithelial layer, while the stroma remained normal. The epithelial layer exhibited improvement; however, it still displayed signs of vacuolation, suggesting partial recovery. The cornea in the diseased group (untreated) exhibited significantly increased thickness of the vacuolated epithelial layer (arrowheads) and pronounced edema in the stroma (thick arrows). This group functions as the negative control, exhibiting significant pathological alterations resulting from infection. The cornea in the healthy control group exhibited a typical arrangement and histological characteristics of the epithelium and stroma, providing a baseline for comparison. The histological evaluation of the cornea indicates that Group 5 offered the most effective treatment, reinstating the cornea to its typical histological appearance. Group 4 demonstrated notable enhancement in both the epithelial layer and stroma. Group 3 demonstrated moderate recovery, yet its efficacy was inferior to that of the optimized formulations. The findings demonstrate the improved therapeutic efficacy of Group 5 in the treatment of corneal infections and the restoration of normal histology.[93,94]

As shown in Figure 11b, the histological analysis of the ciliary body in rabbit eyes showed that the treatment groups were very different from each other. The normal group had normal histological structure, but the untreated group had

severe inflammation, which was shown by a lot of white blood cells entering the tissue, swelling, and blood vessels getting bigger. When the AmB solution was given, there was a moderate improvement, marked by less leukocytic infiltration, which could still be seen. The improved AmB-Ole, on the other hand, showed strong anti-inflammatory activity with little infiltration of white blood cells and better tissue structure. The group of microneedles loaded with AmB-Ole/MNs had the best results, bringing the ciliary body back to a normal histological state similar to the healthy control. These results show that the microneedle system is better at delivering the drug, reducing inflammation, and repairing tissue integrity. This suggests that it could be a promising way to treat inflammatory conditions in the eyes.[95,96]

As shown in Figure 11c, histological examination of the sclera showed a Group 5 (AmB-Oleosome Microneedles) had restoration of the normal scleral stroma and episclera, which were distinguished by uniformly arranged fibroblasts and orderly aligned collagen fibers. This proves to be the most successful treatment since it shows complete recovery and the restoration of normal histological structure. Group 4 (AmB-Oleosomes) the sclera that showed edema in the episclera but no vascularization or leukocytic infiltration. When compared to both untreated and other treated groups, the overall improvement is significant, even though residual edema still exists. Group 3 (Amphotericin B Solution) the sclera in this group displayed edematous and vascularized episclera accompanied by leukocytic cell infiltration. Although there have been improvements when compared to the untreated group, leukocytic infiltration and vascularization indicate that recovery is still ongoing. The group 2 (Untreated), the sclera of this group showed significant inflammation and pathological changes, as evidenced by the leukocytic cell infiltration within the collagen fibers. Group 1 (healthy control group) demonstrated the sclera of this group set the baseline, showing normal episclera and a scleral stroma with uniformly arranged fibroblasts and orderly aligned collagen fibers. Group 5 produced the most effective treatment, according to the histological evaluation of the sclera, returning the scleral stroma and episclera to their typical histological architecture. Group 4 demonstrated substantial enhancement, with negligible edema persisting. Group 3 facilitated moderate recovery; however, it demonstrated vascularization and leukocytic infiltration, suggesting persistent inflammation. The untreated group (Group 2) exhibited significant pathological alterations, underscoring the necessity of advanced formulations such as AmB-Oleosome Microneedles (G5) for enhanced therapeutic efficacy.[97] While histological examination confirmed that AmB-Ole/MNs provided better short-term restoration of normal corneal architecture than free AmB, the long-term effects on corneal healing have yet to be fully assessed. Future studies will include extended follow-up periods to assess stromal remodeling, epithelial integrity, and restoration of corneal transparency, which are essential parameters for confirming total tissue recovery and clinical safety.

Conclusion

In this study, oleosomes were created as nanovesicles to deliver amphotericin-B (AmB) to the eyes. A 3^3-full factorial design was used to investigate the effect of different formulation variables on oleosome characteristics. The selected oleosome formulation had small particle size and polydispersity index values, an acceptable ZP, and a spherical morphology. Microneedles with optimized oleosome formulation were used to increase retention time over ocular tissues. Furthermore, antifungal, in vivo ocular tolerance, cytotoxicity, susceptibility testing, biomarkers, and histopathological studies confirmed the non-irritant nature and superior residence on the eye surface of the prepared Amphotericin-B loaded oleosomes incorporated microneedle formulations. In summary, the findings indicate that the prepared AmB-Ole/MNs could have a wide range of therapeutic applications as an ocular delivery carrier for treating ocular fungal infections.

Data Sharing Statement

Data is available on request from the authors.

Ethics Approval

The Research Ethics Committee-Faculty of Pharmacy, Cairo University (REC-FOPCU) serial number (code: PI 3413) has approved protocols for animal handling and experimental procedures. Animal models are among the most important in vivo models for fundamental parameters like drug efficiency, safety, and toxicological studies because these pre-clinical data are necessary before translating into humans. The ARRIVE criteria for animal research were adhered to in using and handling the study's animals.

Informed Consent Statement

Informed consent was obtained from all subjects involved in the study.

Author Contributions

All authors made a significant contribution to the work reported, whether that is in the conception, study design, execution, acquisition of data, analysis and interpretation, or in all these areas; took part in drafting, revising or critically reviewing the article; gave final approval of the version to be published; have agreed on the journal to which the article has been submitted; and agree to be accountable for all aspects of the work.

Funding

This research received no external funding.

Disclosure

The authors declare no conflicts of interest.

References

1. Hu J, Zhang D, Chen S, et al. Minimally invasive treatment of fungal keratitis with voriconazole microneedle corneal patch. *Eur J Pharm Biopharm*. 2025;211:114717.
2. Nowik KE, Wylęgała A, Nowik K, Wylęgała E. A single-centre retrospective observational study of fungal keratitis in Poland with a review of findings in Europe. *Ann Agric Environ Med*. 2020;27(3):343–347. doi:10.26444/aaem/109414
3. Roy G, Galigama RD, Thorat VS, et al. Amphotericin B containing microneedle ocular patch for effective treatment of fungal keratitis. *Int J Pharm*. 2019;572. doi:10.1016/j.ijpharm.2019.118808
4. Elhabal SF, El-Nabarawi M, Elrefai MFM, et al. Nano-spanlastics-loaded dissolving microneedle patches for ketotifen fumarate: advanced strategies for allergic conjunctivitis treatment and molecular insights. *Drug Deliv Transl Res*. 1–24. Available from: https://link.springer.com/article/10.1007/s13346-025-01796-x. Accessed May 5, 2025
5. Successful management of a refractory scedosporium (pseudallescheria) boydii keratitis with sclerokeratoplasty. *Exp Clin Transplant*. 23:3. Available from: https://pubmed.ncbi.nlm.nih.gov/40223389/. Accessed May 5, 2025
6. Rapti C, Luciano FC, Anaya BJ, et al. Amphotericin B ocular films for fungal keratitis and a novel 3d-printed microfluidic ocular lens infection model. *J Fungi*. 10;11. Available from: http://www.ncbi.nlm.nih.gov/pubmed/39590681. Accessed May 5, 2025
7. Moghadam S, Zarrinfar H, Naseri A, Sadeghi J, Najafzadeh MJ, Heydarian R. Investigating the susceptibility profiles and in vitro combinations of caspofungin, itraconazole, fluconazole, voriconazole, clotrimazole, and amphotericin B against clinical isolates causing fungal keratitis. *Diagn Microbiol Infect Dis*. 2025;112(3). doi:10.1016/j.diagmicrobio.2025.116806
8. Liu X, Zhang Y, Peng F, et al. Macrophage membrane-coated nanoparticles for the delivery of natamycin exhibit increased antifungal and anti-inflammatory activities in fungal keratitis. *ACS Appl Mater Interfaces*. 2024;16(44):59777–59788.
9. Sha X, Chan L, Fan X, et al. Thermosensitive tri-block polymer nanoparticle-hydrogel composites as payloads of natamycin for antifungal therapy against fusarium solani. *Int J Nanomed*. 2022;17:1463–1478. doi:10.2147/IJN.S332127
10. Maciel-Magalhães M, Medeiros RJ, Do C GNC, et al. Amphotericin B encapsulation in polymeric nanoparticles: toxicity insights via cells and zebrafish embryo testing. *Pharmaceutics*. 2025;17(1). doi:10.3390/pharmaceutics17010116
11. Burhanuddin H, Enggi CK, Tangdilintin F, et al. Development of amphotericin B inclusion complex formulation in dissolvable microarray patches for intravaginal delivery. *Daru*. 2024;33(1):5.
12. López-Arencibia A, Bethencourt-Estrella CJ, Berenguer D, et al. In vivo evaluation of sepigel-based meglumine antimoniate and amphotericin b for cutaneous leishmaniasis treatment. *Pathogens*. 2024;13(8). doi:10.3390/pathogens13080712
13. Carvalho-Gondim F, Suzuki ÉY, Rossi-Bergmann B, de J S-BA. Local necrosis induced by intralesional treatment with amphotericin B-deoxycholate. *Acta Trop*. 2025;264. doi:10.1016/j.actatropica.2025.107581
14. Chen Y, Liu F, Jin Q. Polymer-mediated delivery of amphotericin B for fungal infections. *Macromol Rapid Commun*. Available from: https://pubmed.ncbi.nlm.nih.gov/40107872/. Accessed May 05, 2025
15. Das B, Nayak AK, Mallick S. Fluconazole-loaded hyaluronic acid-modified transfersomal hydrogels containing d-panthenol for ocular delivery in fungal keratitis management. *Curr Drug Deliv*. 22. Available from: https://pubmed.ncbi.nlm.nih.gov/39428929/. Accessed May 05, 2025
16. Zarif Attalla K, Hassan DH, Teaima MH, et al. Enhanced intranasal delivery of atorvastatin via superparamagnetic iron-oxide-loaded nanocarriers: cytotoxicity and inflammation evaluation and in vivo, in silico, and network pharmacology study for targeting glioblastoma management. *Pharmaceuticals*. 2025;18(3):421.
17. Elhabal SF, El-Nabarawi MA, Abdelaal N, et al. Development of canagliflozin nanocrystals sublingual tablets in the presence of sodium caprate permeability enhancer: formulation optimization, characterization, in-vitro, in silico, and in-vivo study. *Drug Deliv*. 2023;30(1).
18. Berger BA, Vietor HM, Scott DW, et al. Physicochemical properties of seed oil blends and their potential for the creation of synthetic oleosomes with modulated polarities. *ACS Omega*. 9;42. Available from: https://pubmed.ncbi.nlm.nih.gov/39464465/. Accessed May 5, 2025
19. Frendi S, Chassac A, Veron K, et al. Protective role of oleic acid against palmitic acid-induced pancreatic fibrosis. *J Transl Med*. 2025;23(1):416.
20. Kishida Y, Sakaguchi M, Kunishige T, et al. Disseminated fusariosis successfully treated with empirical liposomal amphotericin B and voriconazole combination followed by ocular therapy in an allogenic hematopoietic stem cell transplant recipient. *Intern Med*. Available from: https://pubmed.ncbi.nlm.nih.gov/40222926/. Accessed May 5, 2025

21. Lee C, Barnett J, Reaven PD. Liposomes enriched in oleic acid are less susceptible to oxidation and have less proinflammatory activity when exposed to oxidizing conditions Supplementary key words monounsaturated fatty acids polyunsatu-rated fatty acids trans fatty acids vitamin E platelet activating factor lipid peroxidation monocyte adhesion chemotaxis minimally mod-ified low density lipoprotein. *J Lipid Res*. 1998;39:1239–1247.
22. Gebicki JM, Hicks M. Ufasomes are stable particles surrounded by unsaturated fatty acid membranes. *Nature*. 1973;243(5404):232–234. doi:10.1038/243232a0
23. Namani T, Ishikawa T, Morigaki K, Walde P. Vesicles from docosahexaenoic acid. *Colloids Surf B Biointerfaces*. 2007;54(1):118–123. doi:10.1016/j.colsurfb.2006.05.022
24. Ji L, Feng W, Chen H, et al.Rapeseed oleosomes facilitate intestinal lymphatic delivery and oral bioavailability of cannabidiol. *Int J Pharm*. 2025;668:124947. doi:10.1016/j.ijpharm.2024.124947
25. Alkhiro AR, Ghareeb MM. Formulation and evaluation of iornoxicam as dissolving microneedle patch. *Iraqi J Pharm Sci*. 2020;29(1):184–194. doi:10.31351/vol29iss1pp184-194
26. Men Z, Su T, Tang Z, Liang J, Shen T. Tacrolimus nanocrystals microneedle patch for plaque psoriasis. *Int J Pharm*.
27. Wang X, Yue J, Guo S, et al. Dissolving microneedles: a transdermal drug delivery system for the treatment of rheumatoid arthritis. *Int J Pharm*. 2025;671:125206. doi:10.1016/j.ijpharm.2025.125206
28. Roy G, Garg P, Venuganti VVK. Microneedle scleral patch for minimally invasive delivery of triamcinolone to the posterior segment of eye. *Int J Pharm*.
29. Putri RA, Enggi CK, Sulistiawati S, et al. Development of itraconazole ocular delivery system using β-cyclodextrin complexation incorporated into dissolving microneedles for potential improvement treatment of fungal keratitis. *J Biomater Sci Polym Ed*. 2024;35(15):2315–2342.
30. Elhabal SF, Abdelaal N, Al-Zuhairy SA, et al. revolutionizing psoriasis topical treatment: enhanced efficacy through ceramide/phospholipid composite cerosomes co-delivery of cyclosporine and dithranol: in-vitro, ex-vivo, and in-vivo studies. *Int J Nanomed*. 2024;19:19. doi:10.2147/IJN.S442775
31. Mu D, Zhou L, Shi L, et al. Quercetin-crosslinked chitosan nanoparticles: a potential treatment for allergic rhinitis. *Sci Rep*. 202414; 1:4021.
32. Al-Zuhairy SAKS, Elhabal SF, Mohamed Elrefai MF, et al. Polylactic-Co-Glycolic Acid/Alginate/Neem Oil-reduced graphene oxide as a pH-sensitive nanocarrier for hesperidin drug delivery: antimicrobial and acute otitis media assessments. *Pharmaceuticals*. 2025;18(3):381.
33. Ezquer-Garin C, Aguilar G, Ferriols-Lisart R, Alos-Almiñana M. Validated HPLC-UV method for amphotericin B quantification in a critical patient receiving AmBisome and treated with extracorporeal replacement therapies. *Biomed Chromatogr*. 2023;37(12). doi:10.1002/bmc.5749
34. Alam SD, Beg MA, Bagadi M, et al. Facile extraction of berberine from different plants, separation, and identification by thin-layer chromatography, high-performance liquid chromatography, and biological evaluation against Leishmaniosis. *J Sep Sci*. 2023;46(21). doi:10.1002/jssc.202300582
35. Elhabal SF, Abdelmonem R, El nashar RM, et al. Enhanced antibacterial activity of clindamycin using molecularly imprinted polymer nanoparticles loaded with polyurethane nanofibrous scaffolds for the treatment of acne vulgaris. *Pharmaceutics*. 2024;16(7):947.
36. ELhabal SF, El-Nabarawi MA, Hassanin SO, et al. Transdermal fluocinolone acetonide loaded decorated hyalurosomes cellulose acetate/polycaprolactone nanofibers mitigated Freund's adjuvant-induced rheumatoid arthritis in rats. *J Pharm Investig*. 2024.
37. Fathy Elhabal S, El-Nabarawi MA, Abdelaal N, et al. Development of canagliflozin nanocrystals sublingual tablets in the presence of sodium caprate permeability enhancer: formulation optimization, characterization, in-vitro, in silico, and in-vivo study. *Drug Deliv*. 2023;30(1). doi:10.1080/10717544.2023.2241665
38. El-Nawawy TM, YomnaA A, Teaima M, et al. Intranasal bilosomes in thermosensitive hydrogel: advancing desvenlafaxine succinate delivery for depression management. *Pharm Dev Technol*. 1–36. Available from: https://pubmed.ncbi.nlm.nih.gov/38965754/. Accessed May 5, 2025
39. Al-Shoubki AA, Teaima MHM, Abdelmonem RAAB, El-Nabarawi MA, Elhabal SF. Potential application of sucrose acetate isobutyrate, and glyceryl monooleate for nanonization and bioavailability enhancement of rivaroxaban tablets. *Pharmaceutical Sci Adv*. 2024;2.
40. Seth R, Meena A, Gosai A, Imam MW, Meena R, Luqman S. Novel nanoformulation for enhanced amphotericin B efficacy and sustained release using vetiver root cellulose nanofibers against Candida albicans. *Int J Biol Macromol*. 2024;282(Pt 2). doi:10.1016/j.ijbiomac.2024.136555
41. Mohanty DL, Divya N, Zafar A, et al. Development of etoricoxib-loaded mesoporous silica nanoparticles laden gel as vehicle for transdermal delivery: optimization, ex vivo permeation, histopathology, and in vivo anti-inflammatory study. *Drug Dev Ind Pharm*. 1–16. Available from: https://pubmed.ncbi.nlm.nih.gov/40192336/. Accessed May 5, 2025.
42. Wang Y, Zheng Y, Zhang L, Wang Q, Zhang D. Stability of nanosuspensions in drug delivery. *J Control Release*. 2013;172(3):1126–1141. doi:10.1016/j.jconrel.2013.08.006
43. ban MMAS, Fitri AMN, Elim D, et al. Combination of synthetic and natural polymers on the characteristics and evaluation of transdermal hydrogel-forming microneedles preparations integrated with direct compressed tablets reservoir sildenafil citrate. *J Drug Deliv Sci Technol*. 2023;85. doi:10.1016/j.jddst.2023.104576
44. Gade S, Glover K, Mishra D, et al. Hollow microneedles for ocular drug delivery. *J Control Release*. 2024;371:43–66. doi:10.1016/j.jconrel.2024.05.013
45. Li Q, Yu X, Zheng X, Yang J, Hui J, Fan D. Rapid dissolution microneedle based on polyvinyl alcohol/chitosan for local oral anesthesia. *Int J Biol Macromol*.
46. Mohammed MHH, Hamed ANE, Elhabal SF, et al. Chemical composition and anti-proliferative activities of Hyophorbe lagenicaulis aerial parts and their biogenic nanoparticles supported by network pharmacology study. *S Afr J Bot*. 2023;156:398–410. doi:10.1016/j.sajb.2023.03.018
47. Rad ZF, Nordon RE, Anthony CJ, et al. High-fidelity replication of thermoplastic microneedles with open microfluidic channels. *Microsyst Nanoeng*. 2017;3.
48. Yang Y, Li Z, Huang P, et al. Rapidly separating dissolving microneedles with sustained-release colchicine and stabilized uricase for simplified long-term gout management. *Acta Pharm Sin B*. 2023;13(8):3454–3470. doi:10.1016/j.apsb.2023.02.011
49. Arena R, Strazzeri MG, Bianchi T, et al. Hypericum and neem oil for dehisced post-surgical wounds: a randomised, controlled, single-blinded Phase III study. *J Wound Care*. 2022;31(6):492–500.
50. Saady M, Shoman NA, Teaima MHM, RAAB A, El-Nabarawi MA, Elhabal SF. Fabrication of gastro-floating sustained-release etoricoxib and famotidine tablets: design, optimization, in-vitro, and in-vivo evaluation. *Pharm Dev Technol*. 2024;29(5):429–444. doi:10.1080/10837450.2024.2343320

51. Bi Y, Liu J, Wang J, et al. Particle size control and the interactions between drug and stabilizers in an amorphous nanosuspension system. *J Drug Deliv Sci Technol*. 2015;29:167–172. doi:10.1016/j.jddst.2015.07.012
52. Elhabal SF, Al-Zuhairy SA, El-Nabarawi MA, et al. Enhancing photothermal therapy for antibiofilm wound healing: insights from graphene oxide-cranberry nanosheet loaded hydrogel in vitro, in silico, and in vivo evaluation. *Int J Nanomed*. 2024;19:19.
53. Lübtow MM, Oerter S, Quader S, et al. In vitro blood–brain barrier permeability and cytotoxicity of an atorvastatin-loaded nanoformulation against glioblastoma in 2D and 3D models. *Mol Pharm*. 2020;17(6):1835–1847.
54. Almutairi B, Albahser G, Almeer R, et al. Investigation of cytotoxicity apoptotic and inflammatory responses of biosynthesized zinc oxide nanoparticles from ocimum sanctum linn in human skin keratinocyte (Hacat) and human lung epithelial (A549) cells. *Oxid Med Cell Longev*. 2020;2020:1–9. doi:10.1155/2020/1835475
55. SKim S, Layton C, Bancroft JD. Bancroft's theory and practice of histological techniques. 2013;637.
56. Sangnim T, Limmatvapirat S, Nunthanid J, et al. Design and characterization of clindamycin-loaded nanofiber patches composed of polyvinyl alcohol and tamarind seed gum and fabricated by electrohydrodynamic atomization. *Asian J Pharm Sci*. 2018;13(5):450–458.
57. Macrophage membrane-coated nanoparticles for the delivery of natamycin exhibit increased antifungal and anti-inflammatory activities in fungal keratitis – pubMed. Available from: https://pubmed.ncbi.nlm.nih.gov/39467057/. Accessed May 5 2025
58. Elhabal SF, Al-Zuhairy SA, El-Nabarawi M, et al. Enhancing photothermal therapy for antibiofilm wound healing: insights from graphene oxide-cranberry nanosheet loaded hydrogel in vitro, in silico, and in vivo Evaluation. *Int J Nanomed*. 2024;19:12999–13027. doi:10.2147/IJN.S482836
59. Wojnicz D, Tichaczek-Goska D, Korzekwa K, Kicia M, Hendrich AB. Study of the impact of cranberry extract on the virulence factors and biofilm formation by Enterococcus faecalis strains isolated from urinary tract infections. *Int J Food Sci Nutr*. 2016;67(8):1005–1016. doi:10.1080/09637486.2016.1211996
60. Shen T, Yang Z. In vivo and in vitro evaluation of in situ gel formulation of pemirolast potassium in allergic conjunctivitis. *Drug Des Devel Ther*. 2021;15:2099. doi:10.2147/DDDT.S308448
61. Antifungal susceptibility, clinical findings, and biofilm resistance of Fusarium species causing keratitis: a challenge for disease control. *Braz J Microbiol*. 2025;56(1). Available from: https://pubmed.ncbi.nlm.nih.gov/39821607/. Accessed May 5, 2025
62. Fang Y, Zhuo L, Yuan H, Zhao H, Zhang L. Construction of graphene quantum dot-based dissolving microneedle patches for the treatment of bacterial keratitis. *Int J Pharm*. 2023;639. doi:10.1016/j.ijpharm.2023.122945
63. Elhabal SF, Abdelaal N, Al-Zuhairy SAS, et al. Revolutionizing psoriasis topical treatment: enhanced efficacy through ceramide/phospholipid composite cerosomes co-delivery of cyclosporine and dithranol: in-vitro, ex-vivo, and in-vivo studies. *Int J Nanomed*. 2024;19:1163–1187. doi:10.2147/IJN.S443812
64. Elhabal S, Abdelaal N, Saeed Al-Zuhairy S, et al. Green synthesis of zinc oxide nanoparticles from althaea officinalis flower extract coated with chitosan for potential healing effects on diabetic wounds by inhibiting TNF-α and IL-6/IL-1β signaling pathways. *Int J Nanomed*. 2024;19:3045–3070. doi:10.2147/IJN.S455270
65. Suvarna P, Chaudhari P, Birangal S, et al. Voriconazole–cyclodextrin supramolecular ternary complex-loaded ocular films for management of fungal keratitis. *Mol Pharm*. 2022;19(1):258–273. doi:10.1021/acs.molpharmaceut.1c00746
66. Logan A, Pucker AD, Franklin Q, et al. Determining initial ocular comfort differences between 0.7% olopatadine and 0.035% ketotifen fumarate. *Cont Lens Anterior Eye*. 2023;46(2). doi:10.1016/j.clae.2022.101769
67. Verma S, Bhardwaj A, Vij M, Bajpai P, Goutam N, Kumar L. Oleic acid vesicles: a new approach for topical delivery of antifungal agent. *Artif Cells Nanomed Biotechnol*. 2014;42(2):95–101. doi:10.3109/21691401.2013.794351
68. Shoman NA, Saady M, Teaima M, Abdelmonem R, El-Nabarawi MA, Elhabal SF. Merging konjac glucomannan with other copolymeric hydrogels as a cutting-edge liquid raft system for dual delivery of etoricoxib and famotidine. *Drug Deliv*. 30(1).
69. Iturrioz-Rodríguez N, Sampron N, Matheu A. Current advances in temozolomide encapsulation for the enhancement of glioblastoma treatment. *Theranostics*. 2023;13(9):2734–2756. doi:10.7150/thno.82005
70. Al-Shoubki AA, Teaima MH, Abdelmonem R, El-Nabarawi MA, Elhabal SF. Sucrose acetate isobutyrate (SAIB) and glyceryl monooleate (GMO) hybrid nanoparticles for bioavailability enhancement of rivaroxaban: an optimization study. *Pharm Dev Technol*. 2023;28(10):928–938. doi:10.1080/10837450.2023.2274944
71. Fouad SA, Malaak FA, Teaima MH, et al. Novel inhalable nano-based/microparticles for enhanced sustained pulmonary delivery of remdesivir - A patient malleable treatment for coronaviruses infection: in vitro aerosolization, cytotoxicity assays and antiviral activity studies. *J Drug Deliv Sci Technol*. 2024;101(Pt A). doi:10.1016/j.jddst.2024.106170.
72. Al-Shoubki AA, Hassan M, Teaima M, et al. Bioavailability enhancement strategies for rivaroxaban: a noteworthy review. *Int J Appl Pharm*;2023. 33–37. doi:10.22159/ijap.2023v15i6.48839
73. Mohammed MHH, Hamed ANE, Elhabal SF, et al. Metabolic profiling and cytotoxic activities of ethanol extract of Dypsis leptocheilos aerial parts and its green synthesized silver nanoparticles supported by network pharmacology analysis. *S Afr J Bot*. 2023;161:648–665. doi:10.1016/j.sajb.2023.08.026
74. Qu J, Zhang L, Chen Z, et al. Nanostructured lipid carriers, solid lipid nanoparticles, and polymeric nanoparticles: which kind of drug delivery system is better for glioblastoma chemotherapy? *Drug Deliv*. 2016;23(9):3408–3416. doi:10.1080/10717544.2016.1189465
75. Yao C, Liu Z, Yang C, et al. Smart hydrogels with inhomogeneous structures assembled using nanoclay-cross-linked hydrogel subunits as building blocks. *ACS Appl Mater Interfaces*. 2016;8(33):21721–21730.
76. El-Gizawy SA, Osman MA, Ibrahim SF. Effect of cosolvents on the absorptive clearance of ketotifen fumarate from rabbit intestine, in-situ. *J Adv Pharm Res*. 2(3):168–179.
77. Zhou Q, Dong K, Wei M, He B, Gao B. Rolling stone gathers moss: rolling Microneedles Generate Meta Microfluidic Microneedles (MMM). *Adv Funct Mater*. 2024;34(25):2316565. doi:10.1002/adfm.202316565
78. Jin M, Jeon WJ, Lee H, et al. Preparation and evaluation of rapid disintegrating formulation from coated microneedle. *Drug Deliv Transl Res*. 2022;12(2):415–425. doi:10.1007/s13346-021-01046-w
79. V MA, Jakka D, Pragathi SG, et al. Polymer coated polymeric microneedles for intravitreal delivery of dexamethasone. *Exp Eye Res*. 2023;231. doi:10.1016/j.exer.2023.109467
80. Sabbagh F, Kim BS. Ex vivo transdermal delivery of nicotinamide mononucleotide using polyvinyl alcohol microneedles. *Polymers*. 15(9).

81. Elhabal SF, Teaima MH, Shawqiali Y, El-Nabarawi MA, Abdelmonem R, Elfar N. Taste masked cloperastine hydrochloride and rupatadine oral dispersible tablets: formulation design, development, characterization and pharmacokinetics study on wistar rats. *Int J Appl Pharm*. 15(4):191–200.
82. Wu Y, Vora LK, Wang Y, et al. Long-acting nanoparticle-loaded bilayer microneedles for protein delivery to the posterior segment of the eye. *Eur J Pharm Biopharm*. 2021;165:306–318. doi:10.1016/j.ejpb.2021.05.022
83. Shen S, Zheng X, Dong X, et al. Methotrexate-loaded hyaluronan-modified liposomes integrated into dissolving microneedles for the treatment of psoriasis. *Eur J Pharm Sci*. 2024;195:106711
84. Datta D, Roy G, Garg P, Venuganti VVK. Ocular delivery of cyclosporine A using dissolvable microneedle contact lens. *J Drug Deliv Sci Technol*.
85. Abdelfattah DSE, Fouad MA, Elmeshad AN, El-Nabarawi MA, Elhabal SF. Anti-obesity effect of combining white kidney bean extract, propolis ethanolic extract and crpi3 on Sprague-Dawley rats fed a high-fat diet. *Nutrients*. 2024;16(2):310. doi:10.3390/nu16020310
86. Araújo KCF, Eula EM, Pazini F, Valadares MC, De Oliveira V. Bioconversion of quercetin and rutin and the cytotoxicity activities of the transformed products. *Food Chem Toxicol*. 2013;51(1):93–96. doi:10.1016/j.fct.2012.09.015
87. Yasser M, El Naggar EE, Elfar N, Teaima MH, El-Nabarawi MA, Elhabal SF. Formulation, optimization and evaluation of ocular gel containing nebivolol Hcl-loaded ultradeformable spanlastics nanovesicles: in vitro and in vivo studies. *Int J Pharm X*. 2024;7. doi:10.1016/j.ijpx.2023.100228
88. Koohestani M, Moradi M, Tajik H, Badali A. Effects of cell-free supernatant of Lactobacillus acidophilus LA5 and Lactobacillus casei 431 against planktonic form and biofilm of Staphylococcus aureus. *Vet Res Forum*. 2018;9(4):301–306. doi:10.30466/vrf.2018.33086
89. Shokri D, Khorasgani MR, Mohkam M, Fatemi SM, Ghasemi Y, Taheri-Kafrani A. The Inhibition effect of lactobacilli against growth and biofilm formation of pseudomonas aeruginosa. *Probiotics Antimicrob Proteins*. 2018;10(1):34–42. doi:10.1007/s12602-017-9267-9
90. Meng Q, Song C, Ma J, et al. Quercetin prevents hyperuricemia associated with gouty arthritis by inactivating the nlrp3/nf-κb signaling pathway. *Chem Biol Drug Des*. 2025;105(4). doi:10.1111/cbdd.70103
91. Aboali FA, Habib DA, Elbedaiwy HM, Farid RM. Curcumin-loaded proniosomal gel as a biofreindly alternative for treatment of ocular inflammation: in-vitro and in-vivo assessment. *Int J Pharm*. 2020;589. doi:10.1016/j.ijpharm.2020.119835
92. Hage-Sleiman R, Mroueh M, Daher CF. Pharmacological evaluation of aqueous extract of Althaea officinalis flower grown in Lebanon. *Pharm Biol*. 2011;49(3):327–333. doi:10.3109/13880209.2010.516754
93. Tavakoli N, Taymouri S, Saeidi A, Akbari V. Thermosensitive hydrogel containing sertaconazole loaded nanostructured lipid carriers for potential treatment of fungal keratitis. *Pharm Dev Technol*. 2019;24(7):891–901. doi:10.1080/10837450.2019.1616755
94. Mahfufah U, Sya'ban Mahfud MA, Saputra MD, et al. Incorporation of inclusion complexes in the dissolvable microneedle ocular patch system for the efficiency of fluconazole in the therapy of fungal keratitis. *ACS Appl Mater Interfaces*. 2024;16(20):25637–25651. doi:10.1021/acsami.3c19482
95. Gaafar PME, Abdallah OY, Farid RM, Abdelkader H. Preparation, characterization and evaluation of novel elastic nano-sized niosomes (ethoniosomes) for ocular delivery of prednisolone. *J Liposome Res*. 2014;24(3):204–215. doi:10.3109/08982104.2014.881850
96. Taghe S, Mirzaeei S, Bagheri M. Preparation of polycaprolactone and polymethacrylate nanofibers for controlled ocular delivery of ketorolac tromethamine: pharmacokinetic study in rabbit's eye. *Eur J Pharm Sci*. 2024;192. doi:10.1016/j.ejps.2023.106631
97. Formica ML, Awde Alfonso HG, Paredes AJ, et al. Development of triamcinolone acetonide nanocrystals for ocular administration. *Pharmaceutics*. 2023;15(2). doi:10.3390/pharmaceutics15020683